

# Exploring the Potential Mechanisms of Guanxinshutong Capsules in Treating Pathological Cardiac Hypertrophy based on Network Pharmacology, Computer-Aided Drug Design, and Animal Experiments

Yuanfeng Liu,<sup>†</sup> Qixiang Li,<sup>†</sup> Chongyu Shao, Yong She, Huifen Zhou, Yan Guo, Huiyan An, Ting Wang, Jiehong Yang,\* and Haitong Wan\*



Cite This: *ACS Omega* 2024, 9, 18083–18098



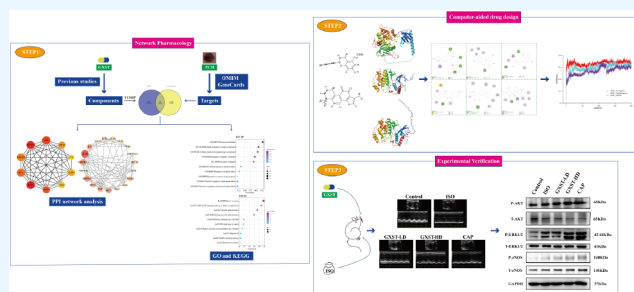
Read Online

ACCESS |

Metrics & More

Article Recommendations

**ABSTRACT:** Cardiovascular diseases (CVDs) are significant causes of morbidity and mortality worldwide, and pathological cardiac hypertrophy (PCH) is an essential predictor of many heart diseases. Guanxinshutong capsule (GXST) is a Chinese patent medicine widely used in the clinical treatment of CVD. In our previous research, we identified 111 compounds of GXST. In order to reveal the potential molecular mechanisms by which GXST treats PCH, this study employed network pharmacology methods to screen for the active ingredients of GXST in treating PCH and predicted the potential targets. The results identified 26 active ingredients of GXST and 110 potential targets for PCH. Through a protein–protein interaction (PPI) network, gene ontology (GO), and Kyoto Encyclopedia of Genes and Genomes (KEGG) analysis, we confirmed AKT1, MAPK1, and MAPK3 as the core proteins in GXST treatment of PCH, thus establishing the PI3K/AKT and MAPK signaling pathways as the significant mechanisms of GXST in treating PCH. The results of molecular docking (MD) demonstrate that flavonoid naringenin and diterpenoid tanshinone iia have the highest binding affinity with the core protein. Before performing molecular dynamics simulations (MDSs), the geometric structure of naringenin and tanshinone iia was optimized using density functional theory (DFT) at the B97–3c level, and RESP2 atomic charge calculations were carried out at the B3LYP-D3(BJ)/def2-TZVP level. Further MDS results demonstrated that in the human body environment, the complex of naringenin and tanshinone iia with core proteins exhibited high stability, flexibility, and low binding free energy. Additionally, naringenin and tanshinone iia showed favorable absorption, distribution, metabolism, excretion, and toxicity (ADMET) characteristics and passed the drug similarity (DS) assessment. Ultrasound cardiograms and cardiac morphometric measurements in animal experiments demonstrate that GXST can improve the PCH induced by isoproterenol (ISO). Protein immunoblotting results indicate that GXST increases the expression of P-eNOS and eNOS by activating the PI3K/AKT signaling pathway and the MAPK signaling pathway, further elucidating the mechanism of action of GXST in treating PCH. This study contributes to the elucidation of the key ingredients and molecular mechanisms of GXST in treating PCH.



## 1. INTRODUCTION

According to statistics from the World Health Organization, CVD has emerged as the predominant cause of mortality associated with noncommunicable diseases globally, and PCH is a risk factor for numerous heart diseases. During the process of postnatal development, cardiac hypertrophy is a common mechanism of cardiac growth. When cardiac function is normal, cardiac hypertrophy is regarded as physiological. When the cardiac function is impaired, cardiac hypertrophy turns into pathological.<sup>1</sup> The main feature of PCH is the enlargement of myocardial cell volume and an increase in cardiac wall thickness, usually resulting from long-term cardiac overload, hypertension, or other cardiac disorders. PCH can result in a

reduction of cardiac contractility, inadequate perfusion to meet the metabolic demands of the body, and ultimately cause heart failure or sudden death.<sup>2</sup> Currently, the treatment of PCH mainly focuses on the causes, such as controlling hypertension, reducing chronic adrenergic receptor stimulation, and restoring heart valve. Additionally, in clinical practice, antihypertensive

**Received:** December 14, 2023

**Revised:** February 15, 2024

**Accepted:** March 8, 2024

**Published:** April 10, 2024



drugs such as ACE inhibitors, diuretics, beta-blockers, and calcium channel blockers are commonly used to improve the symptoms of PCH.<sup>3</sup> These medications have the potential to reduce blood pressure and promote vasodilation, thereby effectively alleviating cardiac hypertrophy. However, long-term use of antihypertensive drugs may lead to drug resistance and side effects such as hypotension, renal impairment, and difficulty breathing. In recent years, safe and effective traditional Chinese herbs have shown potential in the treatment of PCH; commonly used herbs for PCH treatment include *Aconitum carmichaelii* Debeaux, *Hedysarum Multijugum* Maxim, *Radix Salviae*, and *Panax ginseng* C. A. Mey. There are researches showed that knocking out the canonical transient receptor potential channel 1 (TRPC1) can decrease Ca<sup>+</sup> influx and ROS production, thereby exerting a protective effect on the heart.<sup>4,5</sup> The natural compound chlorogenic acid has been demonstrated to protect endothelial cells from LPC-induced injury by attenuating TRPC1 expression.<sup>6</sup> Furthermore, the polysaccharides in *Hedysarum Multijugum* Maxim and *Radix Salviae* also exhibit inhibitory effects on TRPC1,<sup>7,8</sup> providing new directions for research in this field.

Traditional Chinese medicine has been widely used in history due to its multiple pharmacological activities and favorable safety profile. Four different types of Chinese medicines are currently used in preclinical research and clinical treatment of PCH: classic Chinese medicine formulas (such as Zhenwu Tang), patent Chinese medicine (such as Danhong Injection and Shengmai Injection), crude extracts of Chinese herbal medicine (such as Danshen injection), and active components of Chinese herbal medicine (such as Astragaloside IV and tanshinone iia). These Chinese medicines primarily alleviate PCH symptoms through antioxidant and anti-inflammatory effects.<sup>9,10</sup> GXST is a Chinese patent medicine composed of five Chinese herbal medicines, including *Choerospondias axillaris*, *Salvia miltiorrhiza* Bunge, clove, borneol, and *Bambusae concretio* Silicea, with a weight ratio of 16:8:2:1:1, following a prescribed formulation and manufacturing process.<sup>11</sup> In clinical practice, GXST has been used to treat angina pectoris, coronary heart disease, and chronic heart failure.<sup>12–14</sup> Our previous research has indicated that under conditions of pressure overload, GXST significantly inhibits the fibroblasts into including myofibroblasts through the TGF- $\beta$ /Smad3 pathway.<sup>15</sup> Furthermore, during myocardial infarction, GXST has shown positive effects in promoting angiogenesis and protecting myocardial cells.<sup>16</sup> Additionally, using comprehensive analysis, we have identified the presence of flavonoids, diterpenoids, and phenolic acids in GXST ingredients.<sup>17</sup> Although we have made certain achievements in understanding the mechanism of GXST for CVD, further exploration is needed to elucidate the key ingredients and molecular mechanisms underlying its anti-PCH effects.

GXST has a wide range of ingredients, and most of them have been clearly identified. However, the main active ingredients and their effectiveness needs to be further explored; in this study we used network pharmacology and computer-aided drug design to investigate the key ingredients and molecular mechanisms of GXST in combating PCH. In recent years, network pharmacology has become a comprehensive method for understanding the interactions between drugs and biological systems.<sup>18</sup> It has been widely used to elucidate the chemical constituents of herbal medicines and plants as well as their effective mechanisms in diseases, providing new perspectives for research on traditional Chinese

medicine based on complex systems. Zhou et al. explained the active ingredients, targets, and pathways through integrated lipidomics, network pharmacology, and pharmacokinetics to elucidate the therapeutic effects of Eight Zhes Decoction on nonalcoholic fatty liver disease.<sup>19</sup> Computer-aided drug design is a crucial approach in contemporary preclinical drug discovery, and the exponential increase in the number of approved drugs discovered in the past decade can be attributed to various computational techniques. These techniques include molecular docking, DFT, MDS, ADMET prediction, and DS assessment. Molecular docking utilizes scoring functions to assess and rank ligand–receptor complexes, thus, identifying the most probable binding modes. The use of rigorous DFT optimizes the geometric structure of ligands to improve consistency with in vitro experimental results. Besides, MDS can also capture the behavior of proteins and other biomolecules in full atomic detail and at very fine temporal resolution, allowing for the calculation of detailed binding free energies and providing information on the binding mechanisms between small molecules and proteins. Additionally, ADMET prediction and DS assessment can predict the efficacy and effectiveness of candidate key ingredients.<sup>20</sup> Computer-aided drug design plays an essential role in the development of many diseases, such as Alzheimer's disease and COVID-19 infection. Gnanaraj et al. explored the mechanism of action of the natural product karanjin on multiple potential targets in Alzheimer's disease using molecular docking combined with molecular dynamics simulations.<sup>21</sup> Wang et al. used computer-aided drug design combined with network pharmacology to study the targets and mechanisms of Qingfei Paidu Decoction in its antiviral and anti-inflammatory effects against SARS-CoV-2.<sup>22</sup>

The study aims to explore the potential mechanisms of GXST in treating PCH. By using network pharmacology, a “drug ingredient–disease target” network can be constructed to systematically explain the relationship between key components in GXST and its anti-PCH effects. Molecular docking, DFT, and MDS can provide information about the interaction mechanisms between key components and core proteins. Through experimental verification, the therapeutic mechanisms of GXST in treating PCH can be clearly understood. Therefore, our research objective is to identify the key candidate ingredient of GXST for treating PCH and investigate the mechanisms of GXST in treating PCH.

## 2. MATERIALS AND METHODS

**2.1. Database Web Sites and Software.** The databases and software used are as follows: Traditional Chinese Medicine Systems Pharmacology Database (TCMSP; <https://old.tcmsp-e.com/tcmsp.php>), OMIM (<https://www.omim.org/>), GeneCards (<http://www.genecards.org>), Venny2.1.0 (<http://bioinfogp.cnb.csic.es/tools/venny>), UniProt (<https://www.uniprot.org>), STRING (<http://string-db.org/cgi/input.pl>), Metascape (<https://metascape.org/gp/index.html#/main/step1>), Bioinformatics (<https://www.bioinformatics.com.cn/>), CTD (<https://ctdbase.org/>), PubChem (<https://pubchem.ncbi.nlm.nih.gov/>), AlphaFold (<https://www.alphafold.ebi.ac.uk/>), ACPYPE (<https://www.bio2byte.be/acpype/>), PKCSM (<https://biosig.lab.uq.edu.au/pkcsm/>), Cytoscape 3.9.1 software, DruLiTor software, AutoDockTools 1.5.6 software, AutoDock Vina 1.2.3 software, PyMOL 2.5 software, Discovery Studio Visualizer 2021 software, ORCA 5.0.4

software, Multiwfn 3.8 software, Gromacs 2022.2, and Gmx\_MMPBSA software.

**2.2. Network Pharmacology.** **2.2.1. Collection of Active Ingredients and Targets of GXST.** In our previous research, we identified 111 compounds of GXST using high-performance liquid chromatography and mass spectrometry.<sup>17</sup> We screened these 111 compounds based on the following criteria: oral bioavailability (OB)  $\geq$  30% and drug-likeness (DL)  $\geq$  0.18, resulting in the identification of active ingredients in GXST.<sup>23</sup> We further obtained the potential targets of these active ingredients through the TCMSP database.<sup>24</sup> Next, the target names were converted to official symbol format gene targets using the UniProt database.<sup>25</sup> Finally, a active ingredient-target network of GXST active ingredients and their matching targets was constructed using Cytoscape.<sup>26</sup>

**2.2.2. Screening Targets Related to PCH Pathology in GXST.** We searched for targets related to PCH in the OMIM and GeneCards databases.<sup>27,28</sup> When selecting targets, we filtered those with a score  $>8$  based on the GeneCards database.<sup>29</sup> By inputting the keywords 'Pathological cardiac hypertrophy' in both databases, we merged the obtained database targets, eliminated duplicates, and obtained the remaining targets as our desired PCH targets. Subsequently, we used the Venny server to generate a Venn diagram of the targets for GXST and PCH to obtain GXST targets associated with PCH pathology.<sup>30</sup>

**2.2.3. Construction of the PPI Network.** We imported the GXST targets related to PCH into the STRING database and set the organism to "Homo sapiens", and the minimum required interaction score is "highest confidence (0.9)".<sup>31</sup> Subsequently, we used Cytoscape for the visualization of PPI information and constructed a PPI network. To filter the core targets, we used the CytoHubba plugin in Cytoscape to identify hub genes, At the same time, we used the MCODE plugin in Cytoscape to screen modules of the PPI network, setting multiple thresholds such as degree = 2, *k*-core = 2, node score = 0.2, and max depth = 100.<sup>32</sup>

**2.2.4. GO and KEGG Enrichment Analysis.** Using the Metascape server for GO and KEGG enrichment analysis,<sup>33</sup> we identified a series of closely related biological processes, cellular components, and molecular functions, as well as essential signaling pathways involved in GXST treatment of PCH. To better understand these processes and pathways, we uploaded the top 20 terms to the Bioinformatics platform for visualization analysis.<sup>34</sup> Next, through the analysis of the PPI network, GO enrichment analysis, and KEGG pathways, we identified the core proteins involved in the GXST treatment of PCH.

**2.3. Molecular Docking.** Through molecular docking, we explored the binding of key ingredients identified by network pharmacology to core proteins. First, we obtained the three-dimensional structures of the key ingredients from the PubChem database,<sup>35</sup> and the crystal structures of the core proteins from the AlphaFold database.<sup>36,37</sup> Following the method of Li et al.,<sup>38</sup> we used autodockTools to process the three-dimensional structures of the key ingredients and the crystal structures of the core proteins, saving them as PDBQT files for the ligands and receptors, respectively. Subsequently, we performed molecular docking of the ligands and receptors using AutoDock Vina.<sup>39</sup> Using the GetBox plugin in PyMOL, we generated the box parameters and 30 conformations. Finally, we conducted visual analysis with PyMOL and Discovery Studio. During this process, the critical distance

for hydrogen bonding was set to 0.38 nm, and the minimum cutoff angle (Hydrogen–Donor–Acceptor) was 90°.<sup>40</sup>

**2.4. MDS.** After completing molecular docking, Gromacs was used to perform MDS on the selected ligand–receptor complex.<sup>41</sup> The protein's topology was generated using the all-atom force field. At the same time, the small molecule underwent geometric structure optimization at the B97–3c level using the ORCA program, followed by first principle electronic structure calculations at the B3LYP-D3(BJ)/def2-TZVP level.<sup>43</sup> To calculate the RESP2 charges, a combined approach of ORCA and Multiwfn was employed,<sup>44,45</sup> and the topology of small molecule's was constructed using the GAFF force field parameters in the ACPYPE server.<sup>46,47</sup> The TIP3P water model was adopted,<sup>48</sup> and the complex was placed in a dodecahedron box, with the minimum distance between topology of protein atoms and the box edge set to be no less than 1.2 nm.<sup>49</sup> Subsequently, an equilibrated electrolyte solution with an ion concentration of 0.15 M was added to the complex system. Energy minimization was performed by using the steepest descent method until the energy converged to 1000 KJ mol<sup>-1</sup> nm<sup>-1</sup>. The restraint force constants for heavy atoms in both the protein and small molecule were set to 1000 KJ mol<sup>-1</sup> nm<sup>-1</sup>, and the simulation time step was set to 2 fs. Before MDS, all systems were equilibrated under temperature (NVT) and pressure (NPT). First, the temperature was maintained at 310 K using the Berendsen thermostat for NVT equilibration. Then, under isothermal conditions, the pressure was maintained at 1 bar using the Berendsen barostat for NPT equilibration.<sup>50</sup> After constraining the hydrogen bonds in the complex system with the LINCS algorithm,<sup>51</sup> and short-range interactions (Coulomb and van der Waals) had a cutoff of 1.2 nm, a 200 ns MDS simulation was carried out. Finally, various scripts integrated in GROMACS were used to analyze the simulated trajectories.

**2.5. Binding Free Energy Calculation.** To estimate the binding free energy between the ligand and receptor, we employed the molecular mechanics/generalized Born surface area (MM/GBSA) method. We utilized gmx\_MMPBSA to extract the last 20 ns segments of each trajectory for calculation,<sup>52</sup> obtaining the binding free energy between the ligand and receptor, as well as the contribution of each residue to the binding energy. For the calculation of the total binding free energy  $\Delta G_{\text{total}}$ :

$$\Delta G_{\text{total}} = \Delta G_{\text{complex}} - \Delta G_{\text{receptor}} - \Delta G_{\text{ligand}}$$

$$\Delta G_{\text{total}} = \Delta G_{\text{GGAS}} + \Delta G_{\text{GSOLV}}$$

$$\Delta G_{\text{total}} = \Delta G_{\text{VDWAALS}} + \Delta G_{\text{GEEL}} + \Delta G_{\text{GEPB}} + \Delta G_{\text{GESURF}}$$

$\Delta G_{\text{complex}}$  represents the binding free energy of the complex,  $\Delta G_{\text{receptor}}$  represents the free energy of the receptor, and  $\Delta G_{\text{ligand}}$  represents the free energy of the ligand.  $\Delta G_{\text{GGAS}}$  represents the total gas phase free energy, and  $\Delta G_{\text{GSOLV}}$  represents the total solvation free energy.  $\Delta G_{\text{VDWAALS}}$  and  $\Delta G_{\text{GEEL}}$  represent van der Waals and electrostatic energies, respectively.  $\Delta G_{\text{GEPB}}$  and  $\Delta G_{\text{GESURF}}$  represent the polar and nonpolar solvent energies. Due to computational resource limitations, we used the GB model (igb = 8) for calculations,<sup>53</sup> with a salt concentration (saltcon) set to 0.15 M and temperature set to 310 K. Changes in entropy were ignored.

**2.6. ADMET Characteristic Prediction and DS Assessment.** We uploaded the standardized ligand SMILES to the PKCSM server to study ADMET characteristics.<sup>54</sup> Next, we



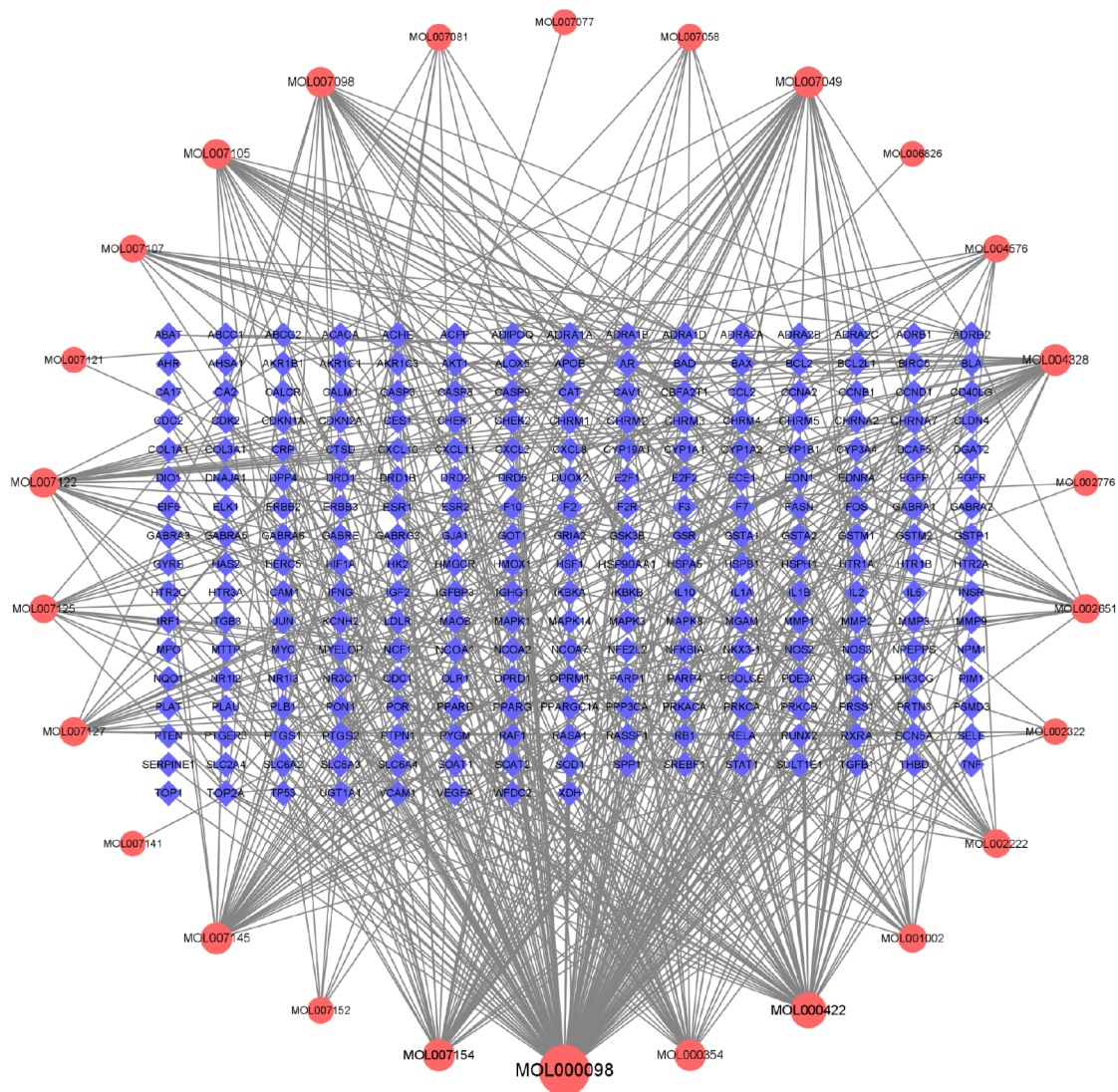


**Figure 1.** Active ingredients and potential targets in GXST. The pink nodes represent the 26 active ingredients of GXST, while the blue nodes represent the 248 potential targets corresponding to the active ingredients. The links between nodes represent the interactions between the active ingredients and potential targets.

used DruLiTor to perform DS assessment on the ligand,<sup>55</sup> predicting its pharmacological properties and its potential as a drug candidate.

**2.7. Animal.** We used 30 Sprague–Dawley rats with body weights ranging from 240 to 280g. These rats were obtained from Shanghai SLAC Laboratory Animal Co., Ltd. (SCXK-(Hu)2022–0004). All animal studies followed the National Institutes of Health Guide for Care and Use of Laboratory Animals and were approved by the Institutional Animal Care and Use Committee of the Laboratory Animal Research Center of Zhejiang Chinese Medical University (approval No.IACUC-202212–19).<sup>56</sup> All rats were housed under appropriate temperature and humidity conditions and provided with a standard diet and free access to water.

**2.8. Chemicals and Medicines.** The Guanxinshutong capsule (Batch number: 220301) was kindly provided by Buchang Pharmaceuticals Co., Ltd. (Xi'an, China). Isoprenaline hydrochloride (Batch number: R015558) was purchased from RHAWN Reagents (Shanghai, China). Captopril tablets (Batch number: 2203101B) were obtained from Zhejiang De En De Pharmaceutical Co, Ltd. (Zhejiang, China). The

Phospho-ERK1/2 (catalog number: ab214036) rabbit monoclonal antibody was purchased from Abcam plc (Cambridge, UK). Phospho-AKT (catalog number: 4060T), Phospho-eNOS (catalog number: 9570S), and anti-eNOS (catalog number: 9586S) rabbit monoclonal antibodies were purchased from Cell Signaling Technology, Inc. (Boston, MA, USA). The anti-ERK1/2 (Cat number: 16443–1-AP) rabbit polyclonal antibody (fusion protein), anti-AKT mouse monoclonal antibody (Cat number: 60203–2-Ig), and anti-GAPDH mouse monoclonal antibody (Cat number: 60004–1-Ig) were purchased from proteintech (Wuhan, China).

**2.9. Experimental Design.** Prior to the start of the experiment, we conducted a 1 week adaptation period for the SD rats in the experimental center. Subsequently, we randomly selected 6 rats as the control group, while the remaining 24 rats were prepared as the model group under sterile conditions by subcutaneous injection of ISO at a dosage of 5 mg/kg for 1 week. The ISO solution was dissolved in physiological saline with a concentration of 10 mg/mL.<sup>57</sup> After observing for 1 week, we performed ultrasound cardiography on the rats, with ejection fraction (EF) as the criterion to evaluate cardiac



function. The rats that successfully developed the model were then randomly divided into four groups, with 6 rats in each group: the ISO group, GXST-LD group (0.5 g/kg/d), GXST-HD group (1.0 g/kg/d), and CAP group (30 mg/kg/d). Based on the animal grouping, we administered oral gavage once daily. The control group and model group received equal volumes of physiological saline. The treatment lasted for 4 weeks, and on the 27th day, we conducted another ultrasound cardiography examination. Within 2 h after the final administration, we anesthetized the rats and extracted their hearts, measured body weight (BW), and tibial length (TL) for subsequent experiments.

**2.10. Echocardiogram.** We performed echocardiographic assessment on rats using the Vevo 1100 system and a 15 MHz transducer (FUJIFILM VisualSonics Inc., Toronto, Canada).<sup>58</sup> Anesthesia was induced by using isoflurane. With guidance from two-dimensional long-axis images, we acquired B-mode and M-mode echocardiograms at the muscle level of the anterior and lateral walls of the left ventricle. All measurements were obtained over at least three consecutive cardiac cycles. Based on the M-mode images, we measured wall thickness and chamber dimensions, and automatically calculated the ejection fraction (EF), end-diastolic interventricular septum thickness (IVSd), posterior wall thickness of the left ventricle (LVPWd), and left ventricular mass (LVMass).

**2.11. Protein Immunoblot Analysis.** First, we extracted cardiac tissue samples and then placed them in a cold RIPA lysis buffer (beyotime biotechnology) containing proteinase and phosphatase inhibitors (bimake). Next, we used a homogenizer to grind the tissue and performed ultrasonic treatment using an ultrasonic disruptor. We centrifuged at 4 °C (12 000 rpm, 10 min) and then determined the total protein content in the supernatant using the BCA protein assay kit (beyotime biotechnology). Subsequently, we balanced the protein content in each group using 4x SDS loading buffer. The tissue protein samples were subjected to electrophoresis in 8%–10% SDS-PAGE (voltage 80–120v), stopping when bromophenol blue reached the bottom to separate total proteins. Then, the constant current wet transfer method was used at 300 mA for 60–90 min. Next, we incubated the membrane with the primary antibody overnight at 4 °C, followed by incubation with the secondary antibody conjugated with horseradish peroxidase (HRP) from the appropriate species (beyotime biotechnology) for 1 h, and finally, we visualized using a chemiluminescent imager (Azure 300).<sup>15</sup> The primary antibodies used included the following: anti-P-ERK1/2 (1:2 000), anti-ERK1/2 (1:2 000), anti-P-AKT (1:2 000), anti-AKT (1:2 000), anti-P-eNOS (1:1 000), anti-eNOS (1:1 000), and GAPDH (1:50 000). Signal results were quantified by using ImageJ software.

**2.12. Statistical Analysis.** Statistical analysis was performed using SPSS software. The results were presented as mean  $\pm$  standard deviation. If the data followed a normal distribution, one-way analysis of variance was used to compare statistical significance. Multiple comparisons after the fact can be conducted using the Tukey test. Differences were considered statistically significant when  $p < 0.05$ .

### 3. RESULTS

**3.1. Network Pharmacology Results.** **3.1.1. Analysis of Active Ingredient-Target Network.** Based on the multi-component and multitarget characteristics of traditional Chinese medicine (TCM) formula, we constructed an active

ingredient-target network of GSXT, which contains 274 nodes and 635 edges. The active ingredients were represented by MOLID and were obtained from the TCMSP database. As shown in Figure 1, the blue diamonds represent the potential targets of GSXT, with a total of 248 potential targets, while the pink circles represent the active ingredients of GSXT, totaling 26 types. Based on the degree values, we ranked the 26 active ingredients of GSXT.

Table 1 shows that the top 10 main ingredients including 4 flavonoid compounds from *Choerospondias axillaris* and *clove*, and 6 diterpenoids compounds from *multiorrhiza Bunge*. The above results indicate that flavonoids and diterpenoid compounds may be the main ingredients of GSXT in treating PCH.

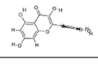
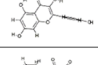
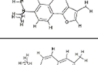
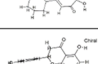
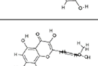
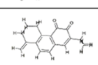
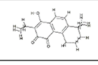
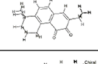
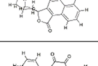
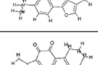
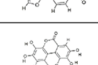
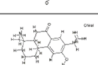
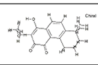
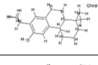
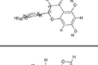
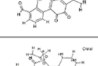
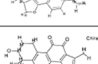
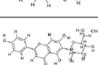
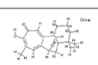
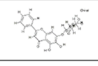
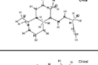
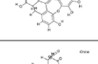
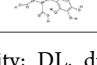
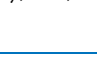
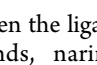
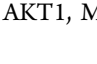
**3.1.2. PPI Network Graph Results.** We obtained 1 177 targets associated with PCH from the OMIM and GeneCard disease databases. According to the Venn diagram results (Figure 2A), GXST shared 110 targets with PCH. To identify the core proteins involved in GXST's treatment of PCH, we imported the information on these shared targets into the STRING database to generate a PPI network. Subsequently, we conducted visualization analysis using Cytoscape. First, the top 10 targets were determined based on the degree value, betweenness centrality, and closeness centrality (Figure 2B). Then, using the CytoHubba plugin in Cytoscape, hub genes were identified by the MCC method (Figure 2C). Finally, the MCODEC plugin in Cytoscape was utilized to screen for network modules with an MCODE score  $>5$  (Figure 2D). The intersections of targets obtained through these three methods included JUN, AKT1, MAPK1, MAPK3, MYC, and ESRI. These potential targets may play a crucial role in the therapeutic effects of GXST on PCH.

**3.1.3. GO Enrichment and KEGG Pathway Results.** After performing GO enrichment analysis, we selected the top 20 results in the Biological Process (BP), Cellular Component (CC), and Molecular Function (MF). The BP analysis mainly involves processes such as response to hormone (GO:0009725), cellular response to nitrogen compound (GO:1901699), and organonitrogen compound (GO:0071417) (Figure 3A). The CC analysis focuses on membrane raft (GO:0045121), membrane microdomain (GO:0098857), and caveola (GO:000590) (Figure 3B). The MF analysis is mainly associated with functions such as DNA-binding transcription factor binding (GO:0140297), transcription factor binding (GO:0008134), and kinase binding (GO:0019900) (Figure 3C).

To further explore the signaling pathway mechanisms of GXST in the treatment of PCH, we conducted KEGG pathway analysis and ranked them based on logP values. Although the cancer pathway (hsa05200) involves a larger number of targets (Figure 3D), considering the results of the GO enrichment analysis and shown in Figure 3E, we found that AKT1, MAPK1, and MAPK3 targets occupy the top three in the top 20 pathways of KEGG analysis. Therefore, we believe that the main mechanisms of GXST in the treatment of PCH may involve the MAPK signaling pathway (hsa04010) and the PI3K/AKT signaling pathway (hsa04151). These results suggest that GXST may potentially treat PCH by modulating proteins AKT1, MAPK1, and MAPK3.

**3.2. Molecular Docking.** To gain a deeper understanding of the binding affinities between core proteins and key ingredients, we utilized AutoDock Vina for molecular docking. In this study, a lower molecular docking score indicates a

Table 1. 26 Active Ingredients of GXST<sup>a</sup>

MOLID	Compound	Molecule structure	Degree	OB	DL	Herb
MOL00098	quercetin		154	46.43	0.28	<i>Choerospondias axillaris</i> , <i>Clove</i>
MOL000422	kaempferol		63	41.88	0.24	<i>Choerospondias axillaris</i> , <i>Clove</i>
MOL007154	tanshinone iia		41	49.89	0.4	<i>Salvia miltiorrhiza</i> Bunge
MOL007145	salviolone		38	31.72	0.24	<i>Salvia miltiorrhiza</i> Bunge
MOL004328	naringenin		37	59.29	0.21	<i>Choerospondias axillaris</i>
MOL000354	isorhamnetin		37	49.6	0.31	N/A
MOL007049	4-methylenemiltirone		33	34.35	0.23	<i>Salvia miltiorrhiza</i> Bunge
MOL007098	deoxyneocryptotanshinone		28	49.4	0.29	<i>Salvia miltiorrhiza</i> Bunge
MOL007122	Miltirone		26	38.76	0.25	<i>Salvia miltiorrhiza</i> Bunge
MOL007105	epidanshenspiroketallactone		26	68.27	0.31	<i>Salvia miltiorrhiza</i> Bunge
MOL002651	1,2-didehydrotanshinone		21	43.76	0.4	<i>Salvia miltiorrhiza</i> Bunge
MOL007127	nortanshinone		20	34.72	0.37	<i>Salvia miltiorrhiza</i> Bunge
MOL001002	ellagic acid		19	43.06	0.43	<i>Choerospondias axillaris</i>
MOL002222	sugiol		17	36.11	0.28	<i>Salvia miltiorrhiza</i> Bunge
MOL007125	neocryptotanshinone		16	52.49	0.32	<i>Salvia miltiorrhiza</i> Bunge
MOL007107	Ferruginol		12	36.07	0.25	<i>Salvia miltiorrhiza</i> Bunge
MOL004576	(+)-taxifolin		11	57.84	0.27	N/A
MOL007058	Formyltanshinone		8	73.44	0.42	<i>Salvia miltiorrhiza</i> Bunge
MOL007081	Danshenol B		8	57.95	0.56	<i>Salvia miltiorrhiza</i> Bunge
MOL007152	tanshindiol C		7	42.85	0.45	<i>Salvia miltiorrhiza</i> Bunge
MOL002322	isovitexin		6	31.29	0.72	N/A
MOL007121	miltipolone		2	36.56	0.37	<i>Salvia miltiorrhiza</i> Bunge
MOL002776	baicalin		2	40.12	0.75	<i>Salvia miltiorrhiza</i> Bunge
MOL007077	sclareol		1	43.67	0.21	<i>Salvia miltiorrhiza</i> Bunge
MOL007141	salvianolic acid G		1	45.56	0.61	<i>Salvia miltiorrhiza</i> Bunge
MOL006826	chebulic acid		1	72	0.32	N/A

<sup>a</sup>OB, oral bioavailability; DL, drug-likeness; N/A, compounds not found in single herb.

higher affinity between the ligand and the receptor. Among the flavonoid compounds, naringenin exhibited the highest docking scores with AKT1, MAPK1, and MAPK3 (compared

to other flavonoids), with scores of  $-7.947$ ,  $-8.223$ , and  $-8.225$  kcal/mol, respectively (Table 2). Regarding the diterpenoid compound tanshinone iia, it showed the highest docking scores with AKT1, MAPK1, and MAPK3 (compared to other diterpenoids), with scores of  $-8.654$ ,  $-9.097$ , and  $-9.306$  kcal/mol, respectively (Table 3). Furthermore, all binding energy scores were below  $-5$  kcal/mol.

As shown in Figure 4, naringenin and tanshinone iia tightly bind to the binding pockets of the core proteins and maintain stability through hydrogen bonding. When naringenin binds to AKT1, it forms hydrogen bonds with amino acid residues GLU191, GLU198, LYS179, and THR195. When binding to MAPK1, it forms a hydrogen bond with amino acid residue LYS54. When binding to MAPK3, it forms hydrogen bonds with amino acid residues LYS71 and MET125 (Figure 4A). In addition, tanshinone iia forms only one hydrogen bond with AKT1, MAPK1, and MAPK3, respectively, with amino acid residues ASP292, LYS114, and LYS71 (Figure 4B). These results suggest that the key components of GXST exhibit strong affinity toward the core proteins.

**3.3. MDS.** **3.3.1. Fluctuations of RMSD, RMSF, Rg and SASA.** Molecular dynamics simulation (MDS) was performed on the complexes of naringenin and tanshinone iia with AKT1, MAPK1, and MAPK3, respectively. The complexes were divided into ligand-protein complex systems (p-L) and independent protein systems (P). Root-mean-square deviation (RMSD) is an important indicator for evaluating the stability and structural similarity of molecular complexes. When the RMSD value is stable, it indicates that the complex system has reached a stable state. Within the AKT1 system, both p-L and P reached a stable state at 20 ns (Figure 5A). In the MAPK1 system, compared to the p-L group, the RMSD of the P group showed larger fluctuations but a smaller average RMSD of  $0.3 \pm 0.04$  nm (Figure 5B). In the MAPK3 system, the RMSD of the tanshinone iia-MAPK3 system showed significant changes but reached stability at 125 ns (Figure 5C). Root-mean-square fluctuation (RMSF) is an important indicator for evaluating the dynamic behavior of each amino acid residue in a complex. It can reveal the stability and activity of each residue during the simulation process. The differences in RMSF values of the amino acid residues in p-L and P in each system were small (Figure 5D–F). Radius of gyration (Rg) is one of the indicators for measuring the compactness of a complex system. A smaller Rg value indicates a more compact structure of the complex. The Rg values of both p-L and P in each system decreased. Specifically, the Rg value of the naringenin-MAPK1 system and P initially decreased and then slightly increased, but the overall trend was a decrease (Figure 5G–I). Solvent-accessible surface area (SASA) describes the area of the complex surface that solvent molecules can contact. A decrease in the SASA value indicates a reduction in the hydrophilic surface area of the complex. The SASA values of both p-L and P in each system decreased significantly (Figure 5J–L). These results indicate that naringenin and tanshinone ii exhibit complex and stable dynamic behavior with core protein complexes during molecular dynamics simulation.

**3.3.2. Combining the Results of Free Energy Calculations.** We calculated the binding free energy of each system using the MM/GBSA method. The highest free energy of binding was observed between naringenin and MAPK3 (compared to other naringenin systems), which was  $-31.39 \pm 4.37$  kcal/mol. Hydrogen bond analysis was performed on the average structures of the last 20 ns, revealing three hydrogen bonds



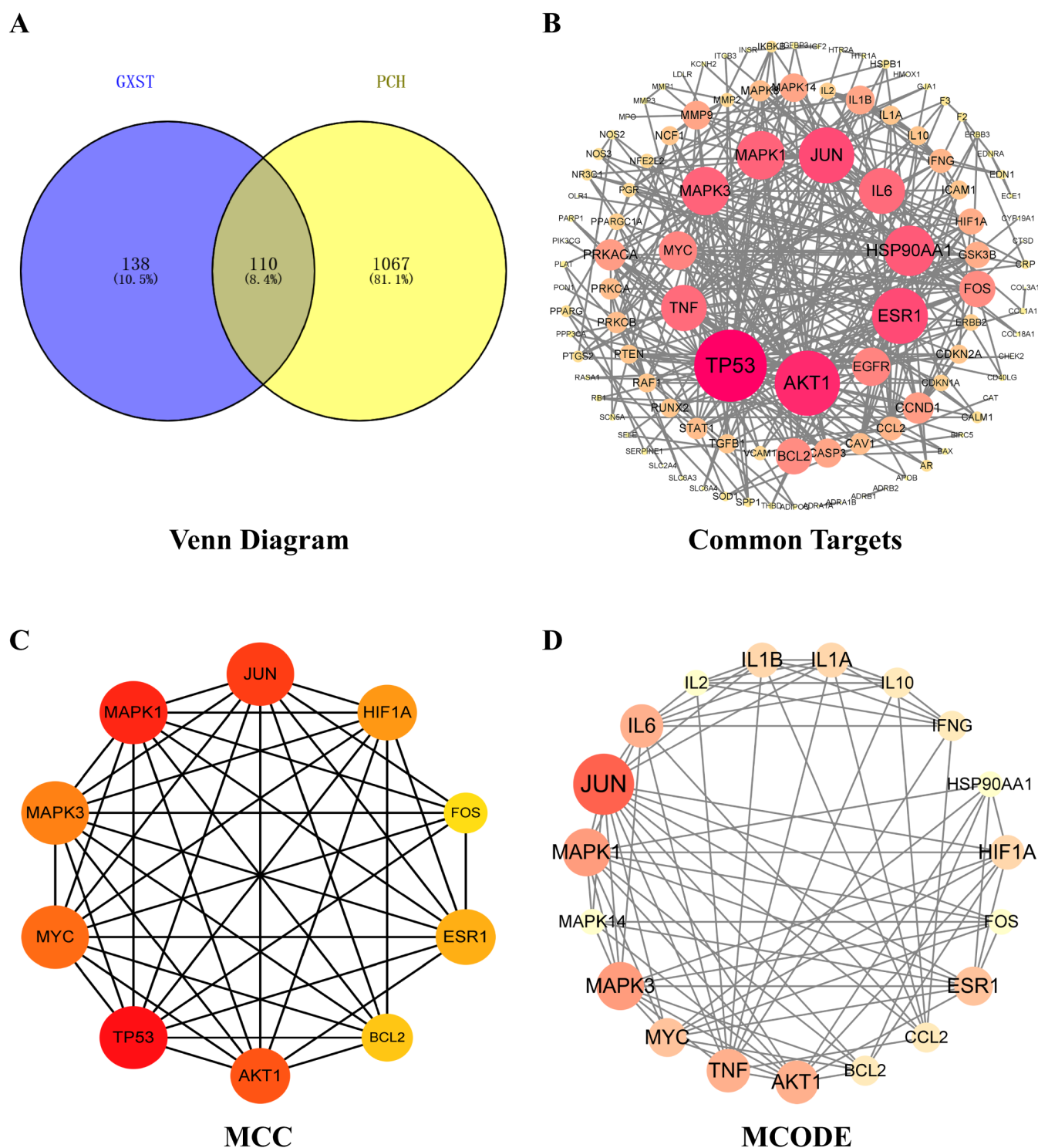


**Figure 2.** A PPI network of the targets for GXST in the treatment of PCH. The intensity of interactions between targets is proportional to the size and color depth of the nodes. Nodes represent targets, and edges indicate interactions between targets. (A) Venn diagram of GXST targets and PCH targets. (B) PPI network of the 110 intersecting targets. (C) Hub genes were identified using the CytoHubba plugin and the MCC method. (D) Network modules with MCODE scores  $>5$ .

(Figure 6A–D). The highest free energy of binding between tanshinone iia and MAPK1 (compared to other tanshinone iia systems) was  $-12.95 \pm 4.01$  kcal/mol. Although no hydrogen bonds were detected, there were significant hydrophobic interactions (Figure 6E–H). These results suggest the presence of specific interactions between naringenin and

tanshinone iii with AKT1, MAPK1, and MAPK3, leading to the formation of stable binding complexes.

**3.4. ADMET and Drug Similarity Results.** To gain a deeper understanding of the pharmacological characteristics of naringenin and tanshinone iii, we utilized the pkCSM server to predict the ADMET properties of naringenin. As shown in Table 4, both naringenin and tanshinone iia exhibit low water

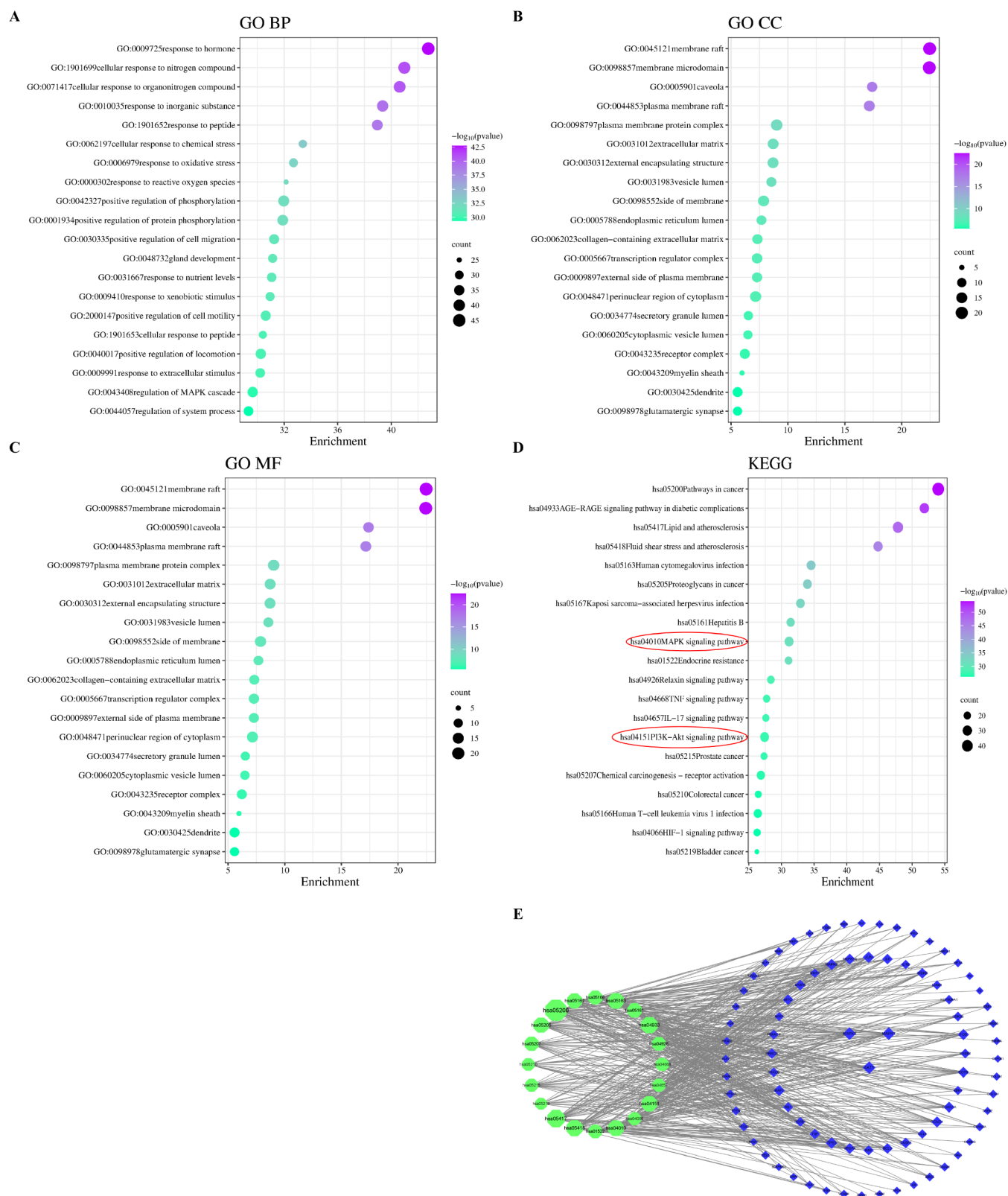


**Figure 3.** Functional enrichment analysis of GXST targets for treating PCH. (A) Bubble chart of the top 20 biological processes revealed by GO enrichment analysis. (B) Related top 20 cellular components. (C) Top 20 molecular functions. (D) Top 20 KEGG pathways. (E) Green nodes represent the top 20 signaling pathways, blue nodes represent the associated targets, and the importance of targets in the top 20 signaling pathways is proportional to the size of the nodes.

solubility in terms of absorption, and their predicted permeability in Caco-2 cells is high, indicating high absorption rates in the human intestinal tract. However, neither

compound easily crosses the blood-brain barrier (BBB) or the central nervous system (CNS), suggesting limited effects on the central nervous system. The cytochrome P450 enzyme



**Table 2. Binding Scores Between KeyFlavonoid Compounds in GXST and Core Proteins**

	AKT1 (kcal/mol)	MAPK1 (kcal/mol)	MAPK3 (kcal/mol)
quercetin	-7.413	-8.213	-7.822
kaempferol	-7.41	-8.07	-7.845
naringenin	-7.948	-8.223	-8.225
isorhamnetin	-7.439	-7.975	-7.917

**Table 3. Binding Scores Between Key Diterpenoid Compounds in GXST and Core Proteins**

	AKT1 (kcal/mol)	MAPK1 (kcal/mol)	MAPK3 (kcal/mol)
tanshinone iia	-8.654	-9.097	-9.306
salviolone	-7.53	-7.66	-7.973
4-methylenemiltirone	-8.373	-8.29	-8.632
deoxyneocryptotanshinone	-8.093	-7.717	-7.783
miltirone	-7.99	-8.156	-8.552
epidanshenspiroketallactone	-8.635	-8.609	-8.847

(CYP) plays a significant role in drug metabolism. We found that naringenin inhibits the CYP1A2 enzyme but has no inhibitory effect on other CYP enzymes. On the other hand, tanshinone iia inhibits the CYP1A2, CYP2C19, and CYP2C9 enzymes. However, tanshinone iia has a higher total clearance rate in the human body compared to that of naringenin. According to the ADMET toxicity parameters, both naringenin and tanshinone iia are considered to have high safety, with no carcinogenic or hepatotoxic effects and no inhibitory effects on hERG I and hERG II. Next, we used DruLiTo to perform a drug score evaluation (DS) for naringenin and tanshinone iia to determine if naringenin can be developed as a drug. As shown in Table 5, we found that both naringenin and

tanshinone iia meet the requirements of Lipinski's Rule, Ghose Filter, and Veber Filter, but fail to pass the MDDR Like Rule. These predictive results indicate favorable parameters for naringenin and tanshinone iii in terms of ADMET properties and DS evaluation.

**3.5. GXST Can Improve PCH Caused by ISO.** After 1 week of ISO model preparation and another week of observation, echocardiography was performed. The results showed that compared to the control group, the EF value of the ISO group significantly decreased (Figure 7A,B). Subsequently, echocardiography was performed 4 weeks after administration. The results showed that compared to the control group, the ISO group had increased IVSd, LVPWd, LVMas, LVMass/BW, and LVMass/TL. Among them, the GXST (different doses) and CAP groups were compared to the ISO group. These values decreased (Figure 7C–H). These data indicate that GXST can improve the ISO-induced PCH.

**3.6. GXST Promotes the Activation of AKT and ERK1/2 Pathways and Increases the Expression and Phosphorylation of eNOS.** Based on network pharmacology and computer-aided drug design methods, we found that GXST may improve PCH by regulating nitrogen and organonitrogen compounds through the PI3K/AKT and MAPK pathways. In order to determine the regulatory mechanism of GXST in treating PCH, the phosphorylation of AKT, ERK1/2, and eNOS was studied. As shown in Figure 8A–E, the protein levels of p-AKT, p-ERK1/2, P-eNOS, and eNOS in the ISO group were higher than those in the normal group ( $p < 0.05$ ). Compared with the ISO group, the protein levels of p-AKT, p-ERK1/2, P-eNOS, and eNOS in the GXST-HD and CAP groups increased more significantly ( $p < 0.05$ ). These results indicate that GXST can improve ISO-induced PCH by activating AKT and MAPK pathways, increasing the expression and phosphorylation of eNOS.

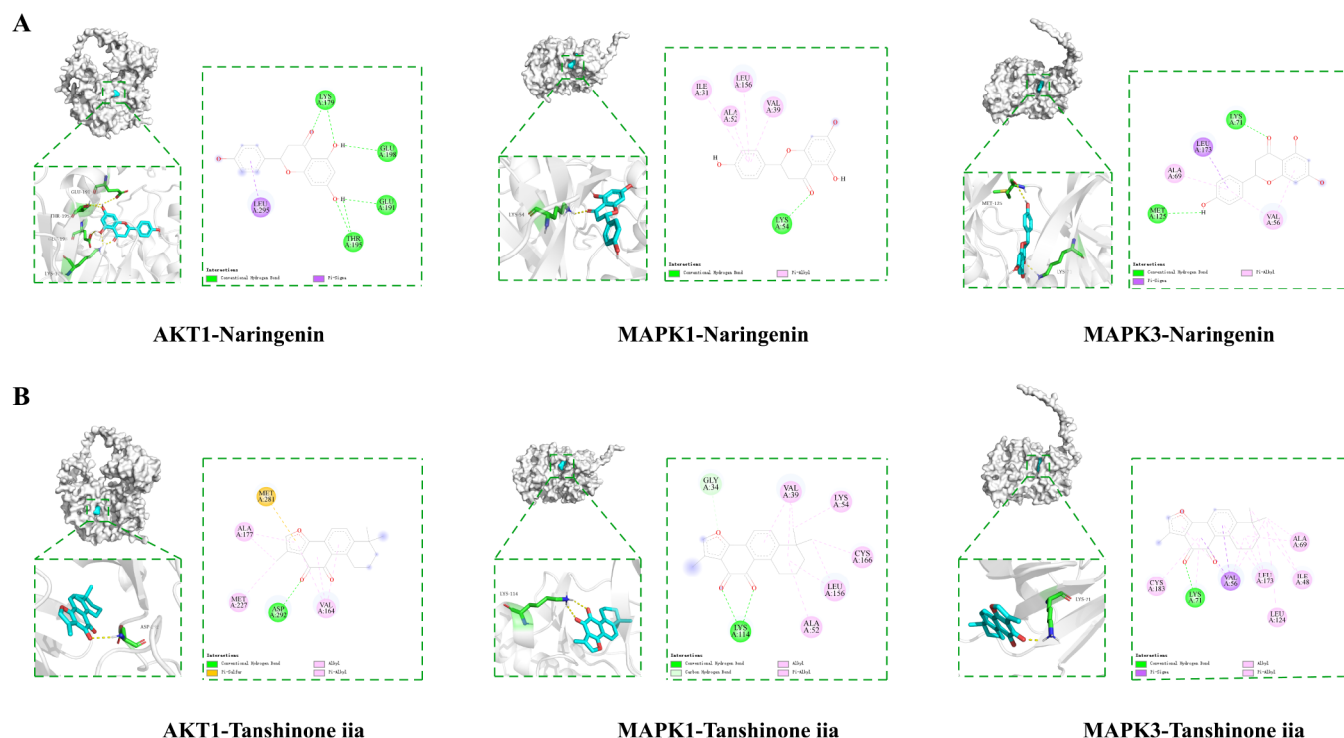


**Figure 4.** Molecular docking of naringenin and tanshinone ii with AKT1, MAPK1, and MAPK3. (A) 3D and 2D binding diagrams of naringenin with AKT1, MAPK1, and MAPK3. (B) 3D and 2D binding diagrams of tanshinone iia with AKT1, MAPK1, and MAPK3.

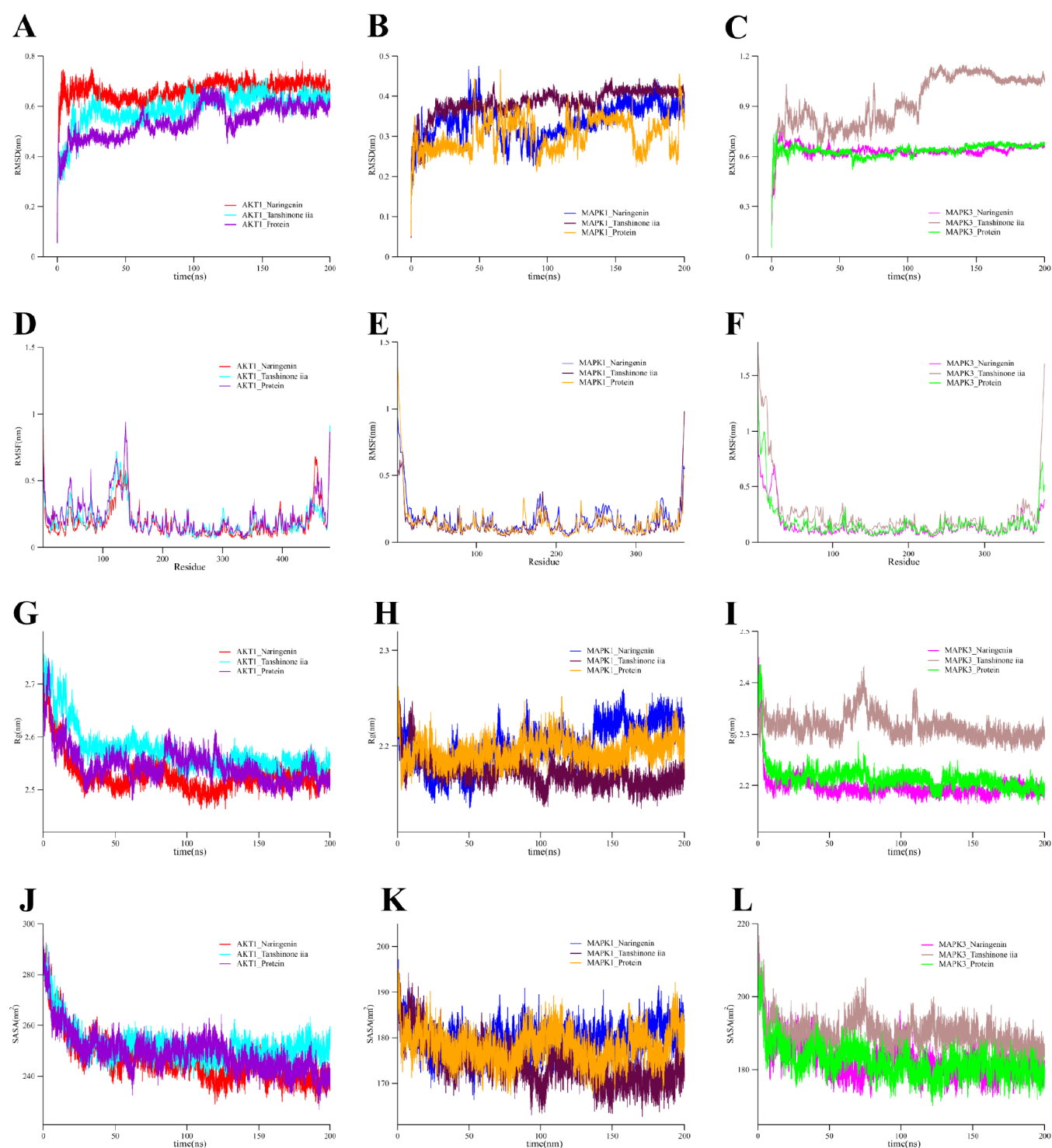


**Figure 5.** Molecular dynamics simulations of naringenin and tanshinone ii with AKT1, MAPK1, and MAPK3 complexes. (A) is the RMSD of the AKT1 system. (B) RMSD of the MAPK1 system. (C) RMSD of the MAPK3 system. (D) RMSF of the AKT1 system. (E) RMSF of the MAPK1 system. (F) RMSF of the MAPK3 system. (G) Rg of the AKT1 system. (H) Rg of the MAPK1 system. (I) Rg of the MAPK3 system. (J) SASA of the AKT1 system. (K) SASA of the MAPK1 system. (L) SASA of the MAPK3 system.

#### 4. DISCUSSION

PCH is an important predictive factor for many cardiovascular diseases. Persistent PCH can lead to impaired systolic function, ultimately causing arrhythmias, heart failure, even sudden death.<sup>59</sup> Currently, drug intervention is primarily used to control PCH, such as widely used with antihypertensive drugs. However, long-term use of antihypertensive drugs may lead to

drug resistance and side effects. Therefore, it is crucial to explore safer and more effective drugs for PCH treatment.

GXST is widely used in the clinical treatment of CVD, Although the therapeutic effect and chemical composition of GXST have been clearly elucidated, the key ingredients and molecular mechanisms in its anti-PCH effects are not fully understood. Therefore, in this study, network pharmacology



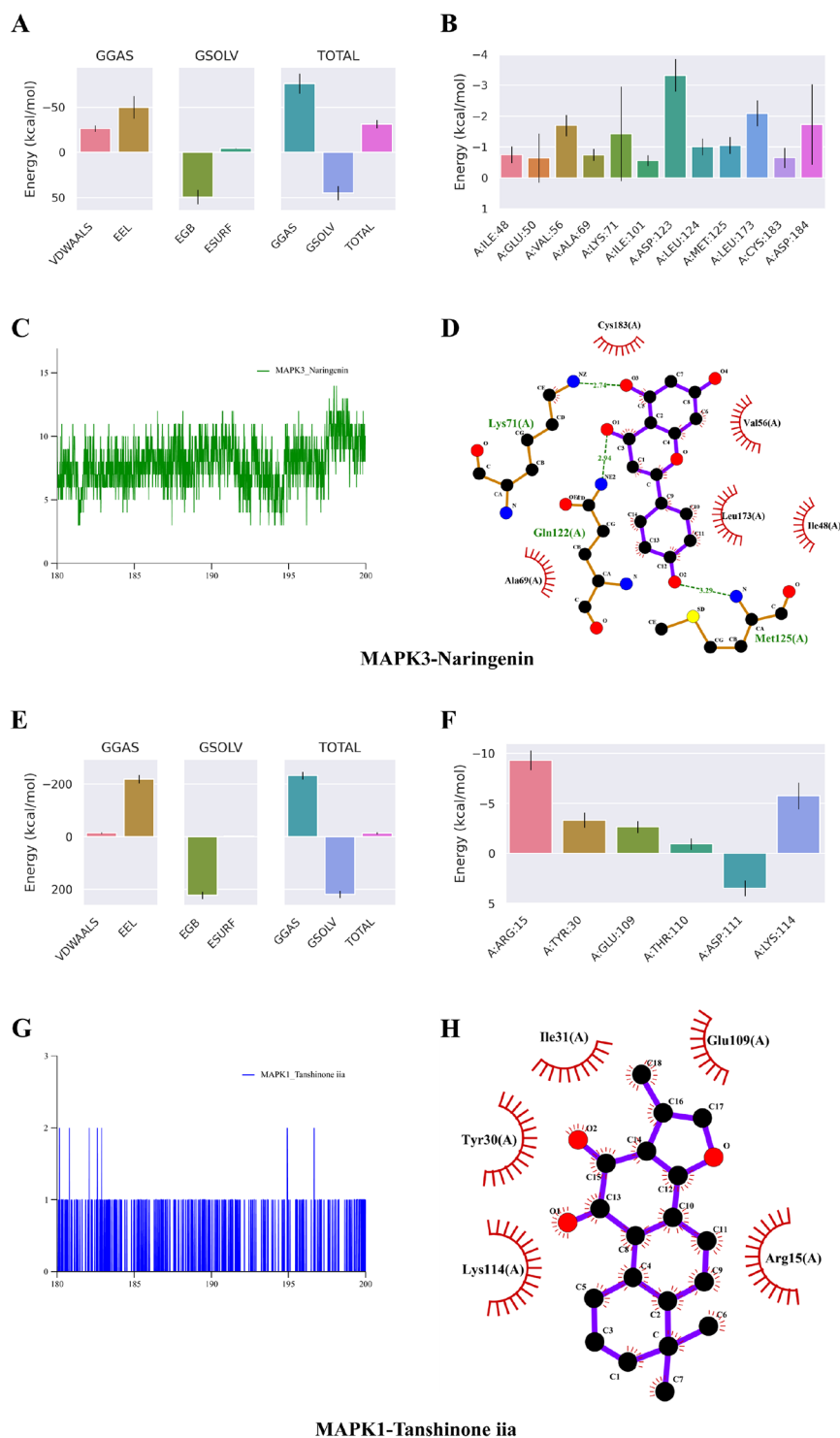


**Figure 6.** Hydrogen bond analysis based on binding free energy analysis and average structures of the last 20 ns. (A) Energy attribute breakdown diagram of MAPK3-naringenin. (B) Energy amino acid decomposition diagram of MAPK3-naringenin. (C) Number of hydrogen bonds in MAPK3-naringenin. (D) 2D representation of the average structure of MAPK3-naringenin. (E) Energy attribute breakdown diagram of MAPK1-tanshinone iia. (F) Energy amino acid decomposition diagram of MAPK1-tanshinone iia. (G) Number of hydrogen bonds in MAPK1-tanshinone iia. (H) 2D representation of the average structure of MAPK1-tanshinone iia. Energy amino acid decomposition was calculated using the TDC-based method. VDWAALS, van der Waals energy; EEL, polar solvation energy; EGB, polar solvation energy; ESURF, nonpolar solvation energy; GGAS, total gas-phase free energy; GSOLV, total solvation free energy; TOTAL, GSOLV + GGAS.

was employed to identify 26 active ingredients and 110 potential targets of GXST. Among the screened active ingredients, flavonoids (kaempferol, naringenin, and quercetin) in *Choerospondias axillaris* had high degrees of nodes,

indicating the important role of total flavonoids in the treatment of PCH, which is consistent with previous research findings. According to reports, total flavonoids of GXST can alleviate cardiac dysfunction and myocardial interstitial fibrosis

**Table 4. Prediction of ADMET Properties of Naringenin**

ADMET		naringenin	tanshinone IIA
absorption	water solubility (log mol/L)	-3.224	-4.494
	Caco2 permeability (log P <sub>app</sub> in 10 <sup>-6</sup> cm/s)	1.029	1.419
	intestinal absorption (human) (%) Absorbed)	91.31	96.253
distribution	BBB permeability (log BB)	-0.578	0.302
	CNS permeability (log PS)	-2.215	-1.494
metabolism	CYP1A2 inhibitor	Yes	Yes
	CYP2C19 inhibitor	No	Yes
	CYP2C9 inhibitor	No	Yes
	CYP2D6 inhibitor	No	No
	CYP3A4 inhibitor	No	No
excretion	total clearance (log mL/min/kg)	0.06	0.821
toxicity	AMES toxicity	No	No
	hERG I inhibitor	No	No
	hERG II inhibitor	No	No
	hepatotoxicity	No	No

by regulating the NF- $\kappa$ B signaling pathway.<sup>60</sup> Another study reported that it can inhibit cyclooxygenase-2 for the treatment of coronary heart disease.<sup>61</sup> Diterpenoids (such as tanshinone iia and miltirone) in *miltiorrhiza* Bunge also had high node degrees and have been extensively studied in the field of cardiovascular disease (CVD) and served as reference standards for GXST.<sup>62</sup> Interestingly, some compounds, such as isorhamnetin, (+)-taxifolin, and isovitexin, were found in GXST but not in individual herbs. These compounds may be formed through chemical reactions of other compounds in the production process. This suggests that GXST, as a Chinese parent medicine, possesses multiple pharmacological activities against PCH, with the main ingredients including flavonoids in *Choerospondias axillaris* and diterpenoids in *Salvia miltiorrhiza* Bunge.

Based on the results of the PPI network, GO enrichment, and KEGG pathways, the core proteins of GXST in the treatment of PCH were identified as AKT1, MAPK1, and MAPK3. These proteins not only have high degrees of nodes but also occupy the top three positions in the top 20 pathways in KEGG. AKT1 is a protein kinase that phosphorylates multiple target proteins, regulating cell proliferation, survival, permeability, nitric oxide release, and cell migration. It is a key kinase effector of the PI3K/AKT signaling pathway. AKT has two downstream signaling branches that largely determine the nature of a given hypertrophy response. One branch activates the mammalian target of rapamycin complex 1 (mTORC1), which is essential for all forms of hypertrophy.<sup>63</sup> The other branch activates glycogen synthase kinase-3 $\beta$  (GSK-3 $\beta$ ), which is one of the earliest discovered negative regulators of cardiac hypertrophy and can block cardiomyocyte hypertrophy.<sup>64</sup> Distinct from physiological hypertrophy, pathological hypertrophy strongly activates the MAPK signaling pathway, and

MAPK1/3 signaling is one of the four classical MAPK signaling pathways, with MAPK1 and MAPK3 sharing 83% sequence identity and most of the same signal activities, also often referred to as ERK1/2.<sup>65</sup> Increasing evidence suggests that ERK1/2 plays a crucial role in the process of PCH. ERK1/2 can phosphorylate over 100 possible substrates and is of great importance in cancer and cardiovascular diseases.<sup>66</sup> ERK1/2 can also activate targets of mTORC1. Previous studies have reported that allicin can simultaneously activate the AKT/mTOR and ERK/mTOR signaling pathways, and alleviate PCH by inhibiting autophagy,<sup>67</sup> indicating that both AKT and ERK1/2 signaling pathways are indispensable in the development of PCH.

In this study, GO BP analysis primarily focused on the response to hormone, cellular response to nitrogen compound, and cellular response to organonitrogen compound. In terms of response to hormone, for example, prolonged exposure of the heart to angiotensin II (Ang II) transforms adaptive or physiological cardiac hypertrophy into maladaptive or pathological hypertrophy.<sup>68</sup> Nitrogen compounds and organonitrogen compounds in the heart play important roles in the development of PCH. Nitric oxide is initially produced by endothelial nitric oxide synthase in the early stage of PCH, and this reaction subsequently leads to the formation of peroxynitrite and produces adverse reactions. At the preclinical level, an increasing body of compelling evidence suggests that reactive oxygen species play a causal role in the occurrence and progression of PCH. Uncoupled nitric oxide synthase and NADPH oxidase are the main sources of reactive oxygen species, and Ang II-induced hypertrophic effects promote ERK1/2, AKT, and NF- $\kappa$ B signaling through NADPH oxidase-dependent reactive oxygen species formation, which is the essential mechanism for inducing myocardial cell hypertrophy.<sup>69</sup> It has also been reported that some natural compounds, such as resveratrol and curcumin, can participate in the alleviation of oxidative stress-induced PCH by modulating the AKT and ERK1/2 signaling pathways.<sup>70,71</sup> These findings indicate that GXST may regulate nitrogen and organonitrogen compounds in the heart through AKT and ERK1/2 signaling to treat PCH.

The molecular docking results show that naringenin and tanshinone iia have the highest score among the core proteins (AKT1, MAPK1, and MAPK3), compared to their respective compound systems. Atomic charges were calculated using RESP2 before conducting MDS for the complexes of naringenin with AKT1, MAPK1, and MAPK3. This calculation is more suitable for nonpolarizable force fields such as GAFF.<sup>44</sup> MDS can simulate the impact of ligand removal on protein conformation by removing the ligands bound to experimentally determined protein structures.<sup>72</sup> The RMSD, Rg, SASA, and RMSF data in the study indicate that each complex system has a high stability in the human body environment.<sup>73</sup> During the MDS process, the hydrogen bonding patterns and hydrophobic interactions are highly consistent with the molecular docking

**Table 5. DS Assessment of Naringenin**

ligand	logP	TPSA	nAtom	MV	HBA	HBD	violations of rule of 5	nRB	lipinski rule <sup>a</sup>	ghose filter <sup>a</sup>	MDDR like rule <sup>a</sup>	VEBER filter <sup>a</sup>	drug likeness alert
naringenin	0.79	86.99	32	272.07	5	3	0	1	+	+	-	+	accept
tanshinone iia	3.247	43.37	40	294.13	3	0	0	0	+	+	-	+	accept

<sup>a</sup>+ indicates meet the requirements and - indicates does not meet the requirements.



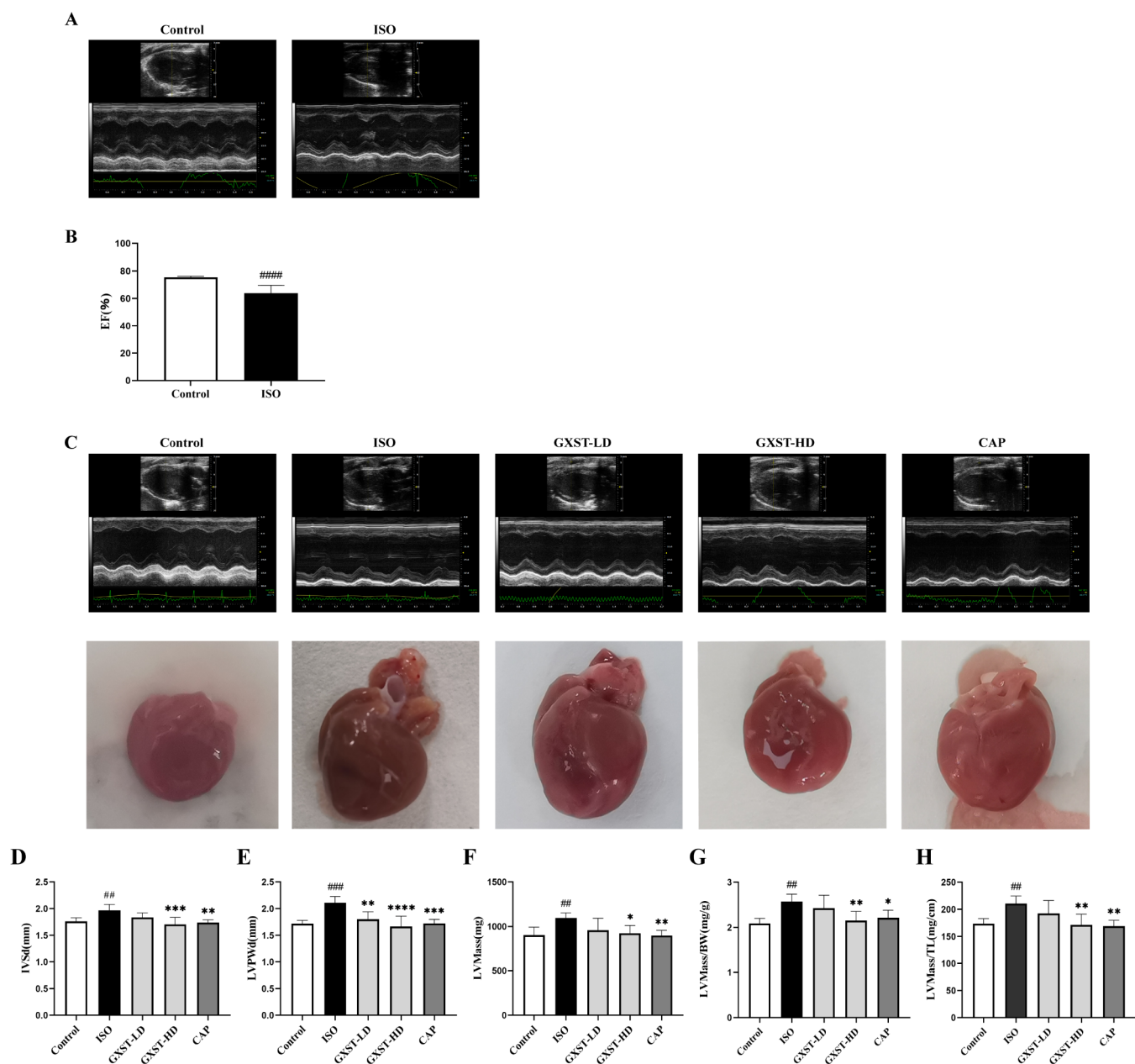


**Figure 7.** GXST alleviated cardiac hypertrophy in vivo in an ISO-induced rat model. Control ( $n = 6$ ) and ISO ( $n = 24$ ) groups were subjected to ISO modeling for 1 week and then underwent echocardiographic examination 1 week later. After 4 weeks of treatment, echocardiographic examination was performed again ( $n = 6$ ). (A) Representative echocardiographic images after modeling. (B) Ejection fraction (EF) after modeling. (C) Representative echocardiographic images and heart images after treatment. (D) Interventricular septal thickness at end-diastole (IVSd). (E) Left ventricular posterior wall thickness at end-diastole (LVPWd). (F) Left ventricular mass (LVMass). (G) Left ventricular mass/body weight (LVMass/BW). (H) Left ventricular mass/tibia length (LVMass/TL). Data are presented as mean  $\pm$  SEM. Differences among groups were analyzed by one-way ANOVA test. # $p < 0.05$ , ## $p < 0.01$  vs normal group, \* $p < 0.05$ , \*\* $p < 0.01$ , \*\*\* $p < 0.001$ , \*\*\*\* $p < 0.0001$  vs ISO group.

results, indicating a high flexibility between the ligands and receptors of each complex. The calculation of the binding free energy demonstrates high affinity between the ligands and receptors of each complex. The predicted ADMET characteristics and DS assessment parameters of naringenin and tanshinone ii are favorable. These results suggest that the binding of naringenin and tanshinone iia with AKT1, MAPK1, and MAPK3 is stable and naringenin and tanshinone iia may improve PCH through multiple targets.

In addition, we confirmed the regulatory effect of GXST on the AKT and ERK pathways through animal experiments. The development of oxidative stress in hypertrophic hearts is an

important mechanism for the transition from cardiac hypertrophy to heart failure. ISO can stimulate  $\beta$ -AR to induce oxidative stress, leading to inflammation and tissue damage.<sup>74</sup> In our study, the expression level of eNOS under GXST treatment was increased, as eNOS can prevent oxidative damage to the heart through regulated NO production. It is worth noting that the increase in eNOS expression is mainly due to the activation of the AKT and ERK pathways, leading to phosphorylation of eNOS, which is crucial for the regulation of eNOS activity and NO production.<sup>75</sup> Therefore, our animal experimental results of ISO-induced PCH confirm the

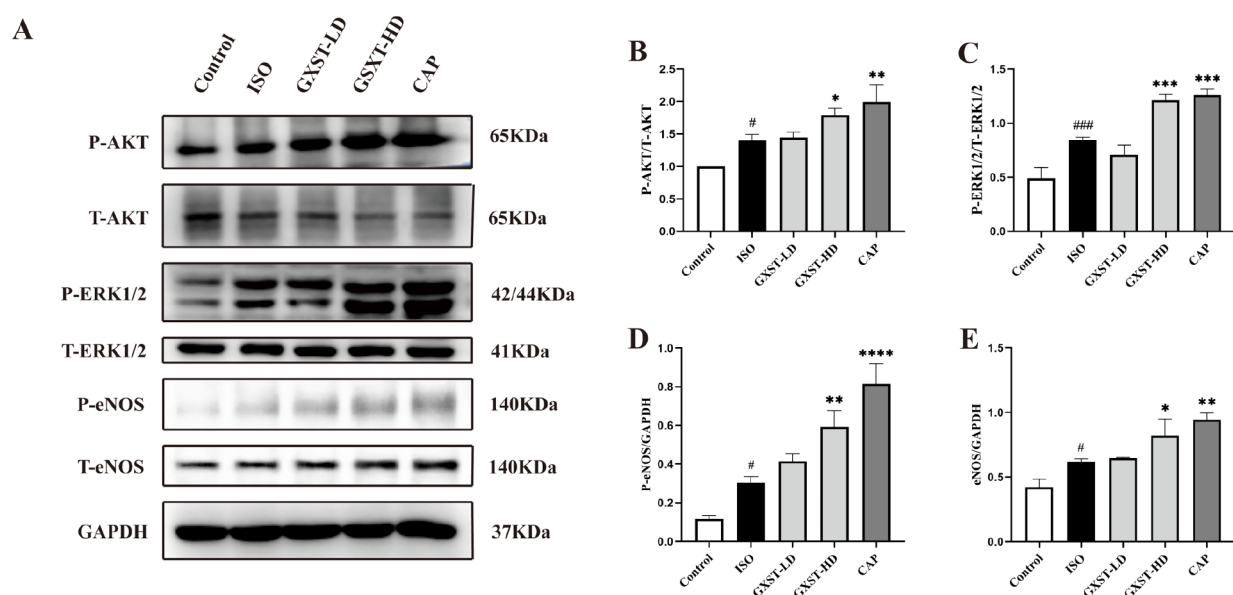


**Figure 8.** GXST activates the AKT and ERK1/2 pathways in the myocardium and increases the expression and phosphorylation of eNOS. (A) Representative immunoblot images of p-AKT, T-AKT, p-ERK1/2, T-ERK1/2, P-eNOS, and eNOS. (B) p-AKT/T-AKT ratio. (C) p-ERK1/2/T-ERK1/2 ratio. (D) P-eNOS/GAPDH ratio. (E) eNOS/GAPDH ratio ( $n = 3$ ). Data are presented as mean  $\pm$  SEM. Differences among groups were analyzed by one-way ANOVA test. # $p < 0.05$ , ### $p < 0.001$  vs normal group, \* $p < 0.05$ , \*\* $p < 0.01$ , \*\*\* $p < 0.001$ , \*\*\*\* $p < 0.0001$  vs ISO group.

pharmacological effect of GXST in inhibiting oxidative stress, revealing the mechanism of GXST in treating PCH.

## 5. CONCLUSION

In summary, network pharmacology, computer-aided drug design, and animal experiments have provided evidence for the potential of GXST to improve PCH by activating the AKT and ERK1/2 signaling pathways, increasing the expression and phosphorylation of eNOS and inhibiting oxidative stress reactions, particularly in the flavonoid naringenin and the diterpenoid tanshinone iia in GXST. These compounds are considered potential drugs for the treatment of PCH with GXST. Our research findings provide scientific evidence for the development and clinical application of GXST in PCH.

## AUTHOR INFORMATION

### Corresponding Authors

**Haitong Wan** – College of Basic Medical Sciences, Zhejiang Chinese Medical University, Hangzhou, Zhejiang 310053, China; Key Laboratory of TCM Encephalopathy of Zhejiang Province, Hangzhou, Zhejiang 310053, China; Email: [whtong@126.com](mailto:whtong@126.com)

**Jiehong Yang** – College of Basic Medical Sciences, Zhejiang Chinese Medical University, Hangzhou, Zhejiang 310053, China; Key Laboratory of TCM Encephalopathy of Zhejiang Province, Hangzhou, Zhejiang 310053, China; Email: [yah8455@126.com](mailto:yah8455@126.com)

### Authors

**Yuanfeng Liu** – College of Life Science, Zhejiang Chinese Medical University, Hangzhou, Zhejiang 310053, China; [orcid.org/0009-0006-4411-4482](https://orcid.org/0009-0006-4411-4482)

**Qixiang Li** – College of Basic Medical Sciences, Zhejiang Chinese Medical University, Hangzhou, Zhejiang 310053, China

**Chongyu Shao** – College of Basic Medical Sciences, Zhejiang Chinese Medical University, Hangzhou, Zhejiang 310053, China

China; Key Laboratory of TCM Encephalopathy of Zhejiang Province, Hangzhou, Zhejiang 310053, China

**Yong She** – College of Life Science, Zhejiang Chinese Medical University, Hangzhou, Zhejiang 310053, China

**Huifan Zhou** – College of Basic Medical Sciences, Zhejiang Chinese Medical University, Hangzhou, Zhejiang 310053, China; Key Laboratory of TCM Encephalopathy of Zhejiang Province, Hangzhou, Zhejiang 310053, China

**Yan Guo** – Hangzhou TCM Hospital Affiliated to Zhejiang Chinese Medical University, Hangzhou, Zhejiang 310053, China

**Huiyan An** – College of Life Science, Zhejiang Chinese Medical University, Hangzhou, Zhejiang 310053, China

**Ting Wang** – College of Basic Medical Sciences, Zhejiang Chinese Medical University, Hangzhou, Zhejiang 310053, China

Complete contact information is available at:

<https://pubs.acs.org/10.1021/acsomega.3c10009>

### Author Contributions

<sup>†</sup>Y.L. and Q.L. contributed equally to this work and share first authorship.

### Notes

The authors declare no competing financial interest.

## ACKNOWLEDGMENTS

This study was funded by the National Key R&D Program [2023YFC3503100] and Key Laboratory of TCM Encephalopathy of Zhejiang Province [2020E10012]. The authors would like to appreciate the technical and instrumental support provided by the Zhejiang Chinese Medical University Laboratory Animal Research Center.

## REFERENCES

(1) Shimizu, I.; Minamino, T. Physiological and pathological cardiac hypertrophy. *J. Mol. Cell. Cardiol.* **2016**, *97*, 245–262.

- (2) Nakamura, M.; Sadoshima, J. Mechanisms of physiological and pathological cardiac hypertrophy. *Nat. Rev. Cardiol.* **2018**, *15* (7), 387–407.
- (3) Martin, T. G.; Juarros, M. A.; Leinwand, L. A. Regression of cardiac hypertrophy in health and disease: mechanisms and therapeutic potential. *Nat. Rev. Cardiol.* **2023**, *20* (5), 347–363.
- (4) Hu, Q.; Ahmad, A. A.; Seidel, T.; Hunter, C.; Streiff, M.; Nikolova, L.; Spitzer, K. W.; Sachse, F. B. Location and function of transient receptor potential canonical channel 1 in ventricular myocytes. *J. Mol. Cell. Cardiol.* **2020**, *139*, 113–123.
- (5) Zhang, H. N.; Zhang, M.; Tian, W.; Quan, W.; Song, F.; Liu, S. Y.; Liu, X. X.; Mo, D.; Sun, Y.; Gao, Y. Y.; et al. Canonical transient receptor potential channel 1 aggravates myocardial ischemia-and-reperfusion injury by upregulating reactive oxygen species. *J. Pharm. Anal.* **2023**, *13* (11), 1309–1325.
- (6) Wang, H.; Cheng, X.; Tian, J.; Xiao, Y.; Tian, T.; Xu, F.; Hong, X.; Zhu, M. X. TRPC channels: Structure, function, regulation and recent advances in small molecular probes. *Pharmacol. Ther.* **2020**, *209*, 107497.
- (7) Zhang, D.; Zhu, Y.; Li, Z.; Luo, M.; Liang, X.; Wang, A.; Zhu, H.; Hu, L.; Li, R. The role of Astragalus polysaccharides in promoting IEC-6 cell migration from polyamine-mediated Ca(2+) regulation. *Int. J. Biol. Macromol.* **2022**, *207*, 179–192.
- (8) Zhu, H.; Cao, J.; Liang, X.; Luo, M.; Wang, A.; Hu, L.; Li, R. Polysaccharides from Panax ginseng promote intestinal epithelial cell migration through affecting the Ca(2+) related regulators. *J. Ginseng Res.* **2023**, *47* (1), 89–96.
- (9) Xu, L.; Chen, L.; Gu, G.; Wang, Y.; Xu, Y.; Zhong, Y. Natural products from traditional Chinese medicine for the prevention and treatment of heart failure: progress and perspectives. *Rev. Cardiovasc. Med.* **2022**, *23* (2), 60.
- (10) Wang, L.; Yu, J.; Fordjour, P. A.; Xing, X.; Gao, H.; Li, Y.; Li, L.; Zhu, Y.; Gao, X.; Fan, G. Danshen injection prevents heart failure by attenuating post-infarct remodeling. *J. Ethnopharmacol.* **2017**, *205*, 22–32.
- (11) Committee, C.. *The 2020 ed. of Pharmacopoeia of the People's Republic of China*. Dandy Booksellers; 2020
- (12) Li, Y.; Zhang, L.; Lv, S.; Wang, X.; Zhang, J.; Tian, X.; Zhang, Y.; Chen, B.; Liu, D.; Yang, J.; et al. Efficacy and safety of oral Guanxinshutong capsules in patients with stable angina pectoris in China: A prospective, multicenter, double-blind, placebo-controlled, randomized clinical trial. *BMC Complementary Altern. Med.* **2019**, *19* (1), 363.
- (13) Cui, X.; Han, S.; Li, J.; Li, W.; Wang, Z. F.; Zhang, Q.; Xie, Y. M. [Clinical comprehensive evaluation of Guanxin Shutong Capsules in treatment of coronary heart disease angina pectoris with heart blood stasis syndrome]. *Zhongguo Zhong Yao Za Zhi* **2022**, *47* (6), 1469–1475.
- (14) Wang, Y.; Xu, J.; Yang, J.; Zhang, L.; Pan, Y.; Dou, L.; Zhou, P.; Xu, Y.; Li, C.; He, Y.; et al. Effects of Guanxinshutong Capsules as Complementary Treatment in Patients With Chronic Heart Failure: Study Protocol for a Randomized Controlled Trial. *Front. Pharmacol.* **2021**, *11*, 571106.
- (15) Pan, Y.; Shao, C.; Zhang, L.; He, Y.; Yang, J.; Fu, W.; Yang, J.; Wan, H. The effect of Guanxin Shutong capsule on alleviating the myocardial fibrosis in heart failure rats. *J. Ethnopharmacol.* **2021**, *275*, 114169.
- (16) Zhu, J.; Zhou, H.; Li, C.; He, Y.; Pan, Y.; Shou, Q.; Fang, M.; Wan, H.; Yang, J. Guanxinshutong capsule ameliorates cardiac function and architecture following myocardial injury by modulating ventricular remodeling in rats. *Biomed. Pharmacother.* **2020**, *130*, 110527.
- (17) Meng, M.; Wan, H.; Bao, Y.; He, Y.; Li, C.; Wan, H. Rapid identification, quantitation, and antioxidant activity evaluation of the components in Guanxin Shutong capsule with liquid chromatography and mass spectrometry. *J. Pharm. Biomed. Anal.* **2023**, *224*, 115194.
- (18) Hopkins, A. L. Network pharmacology. *Nat. Biotechnol.* **2007**, *25* (10), 1110–1111.
- (19) Zhou, Y.; Dai, Z.; Deng, K.; Wang, Y.; Ying, J.; Chu, D.; Zhou, J.; Tang, C. Eight Zhes Decoction ameliorates the lipid dysfunction of nonalcoholic fatty liver disease using integrated lipidomics, network pharmacology and pharmacokinetics. *J. Pharm. Anal.* **2023**, *13* (9), 1058–1069.
- (20) Sabe, V. T.; Ntombela, T.; Jhamba, L. A.; Maguire, G. E. M.; Govender, T.; Naicker, T.; Kruger, H. G. Current trends in computer aided drug design and a highlight of drugs discovered via computational techniques: A review. *Eur. J. Med. Chem.* **2021**, *224*, 113705.
- (21) Niu, Y.; Lin, P. Advances of computer-aided drug design (CADD) in the development of anti-Alzheimer's-disease drugs. *Drug Discovery Today* **2023**, *28* (8), 103665.
- (22) Wang, Z.; Zhan, J.; Gao, H. Computer-aided drug design combined network pharmacology to explore anti-SARS-CoV-2 or anti-inflammatory targets and mechanisms of Qingfei Paidu Decoction for COVID-19. *Front. Immunol.* **2022**, *13*, 1015271.
- (23) Tian, S.; Wang, J.; Li, Y.; Li, D.; Xu, L.; Hou, T. The application of in silico drug-likeness predictions in pharmaceutical research. *Adv. Drug Delivery Rev.* **2015**, *86*, 2–10.
- (24) Ru, J.; Li, P.; Wang, J.; Zhou, W.; Li, B.; Huang, C.; Li, P.; Guo, Z.; Tao, W.; Yang, Y.; et al. TCMSP: a database of systems pharmacology for drug discovery from herbal medicines. *J. Cheminf.* **2014**, *6*, 13.
- (25) The UniProt Consortium. UniProt: The universal protein knowledgebase. *Nucleic Acids Res.* **2018**, *46* (5), 2699.
- (26) Shannon, P.; Markiel, A.; Ozier, O.; Baliga, N. S.; Wang, J. T.; Ramage, D.; Amin, N.; Schwikowski, B.; Ideker, T. Cytoscape: a software environment for integrated models of biomolecular interaction networks. *Genome Res.* **2003**, *13* (11), 2498–2504.
- (27) Amberger, J. S.; Bocchini, C. A.; Schiettecatte, F.; Scott, A. F.; Hamosh, A. OMIM.org: Online Mendelian Inheritance in Man (OMIM®), an online catalog of human genes and genetic disorders. *Nucleic Acids Res.* **2015**, *43*, D789–D798.
- (28) Safran, M.; Dalah, I.; Alexander, J.; Rosen, N.; Stein, T. I.; Shmoish, M.; Nativ, N.; Bahir, I.; Doniger, T.; Krug, H.; et al. GeneCards Version 3: The human gene integrator **2010**, 2010, baq020.
- (29) He, Y. Y.; Xie, X. M.; Zhang, H. D.; Ye, J.; Gencer, S.; van der Vorst, E. P. C.; Döring, Y.; Weber, C.; Pang, X. B.; Jing, S. C.; et al. Identification of Hypoxia Induced Metabolism Associated Genes in Pulmonary Hypertension. *Front. Pharmacol.* **2021**, *12*, 753727.
- (30) Oliveros, J. C.. *Venny. An interactive tool for comparing lists with Venn Diagrams*, CiNii, 2007.
- (31) Szklarczyk, D.; Morris, J. H.; Cook, H.; Kuhn, M.; Wyder, S.; Simonovic, M.; Santos, A.; Doncheva, N. T.; Roth, A.; Bork, P.; et al. The STRING database in 2017: quality-controlled protein–protein association networks, made broadly accessible. *Nucleic Acids Res.* **2017**, *45* (D1), D362–D368.
- (32) Shen, M.; Duan, C.; Xie, C.; Wang, H.; Li, Z.; Li, B.; Wang, T. Identification of key interferon-stimulated genes for indicating the condition of patients with systemic lupus erythematosus. *Front. Immunol.* **2022**, *13*, 962393.
- (33) Zhou, Y.; Zhou, B.; Pache, L.; Chang, M.; Khodabakhshi, A. H.; Tanaseichuk, O.; Benner, C.; Chanda, S. K. Metascape provides a biologist-oriented resource for the analysis of systems-level datasets. *Nat. Commun.* **2019**, *10* (1), 1523.
- (34) Chen, Y.; Gan, Y.; Yu, J.; Ye, X.; Yu, W. Key ingredients in Verbena officinalis and determination of their anti-atherosclerotic effect using a computer-aided drug design approach. *Front. Plant Sci.* **2023**, *14*, 1154266.
- (35) Kim, S.; Chen, J.; Cheng, T.; Gindulyte, A.; He, J.; He, S.; Li, Q.; Shoemaker, B. A.; Thiessen, P. A.; Yu, B.; et al. PubChem in 2021: New data content and improved web interfaces. *Nucleic Acids Res.* **2021**, *49* (D1), D1388–D1395.
- (36) Jumper, J.; Evans, R.; Pritzel, A.; Green, T.; Figurnov, M.; Ronneberger, O.; Tunyasuvunakool, K.; Bates, R.; Židek, A.; Potapenko, A.; et al. Highly accurate protein structure prediction with AlphaFold. *Nature* **2021**, *596* (7873), 583–589.



- (37) Varadi, M.; Anyango, S.; Deshpande, M.; Nair, S.; Natassia, C.; Yordanova, G.; Yuan, D.; Stroe, O.; Wood, G.; Laydon, A.; et al. AlphaFold Protein Structure Database: massively expanding the structural coverage of protein-sequence space with high-accuracy models. *Nucleic Acids Res.* **2022**, *50* (D1), D439–D444.
- (38) Li, X.; Wei, S.; Niu, S.; Ma, X.; Li, H.; Jing, M.; Zhao, Y. Network pharmacology prediction and molecular docking-based strategy to explore the potential mechanism of Huanglian Jiedu Decoction against sepsis. *Comput. Biol. Med.* **2022**, *144*, 105389.
- (39) Trott, O.; Olson, A. J. AutoDock Vina: improving the speed and accuracy of docking with a new scoring function, efficient optimization, and multithreading. *J. Comput. Chem.* **2010**, *31* (2), 455–461.
- (40) Lee, S.; Wong, A. R.; Yang, A. W. H.; Hung, A. Interaction of compounds derived from the Chinese medicinal formula Huangqi Guizhi Wuwu Tang with stroke-related numbness and weakness targets: An in-silico docking and molecular dynamics study. *Comput. Biol. Med.* **2022**, *146*, 105568.
- (41) Van Der Spoel, D.; Lindahl, E.; Hess, B.; Groenhof, G.; Mark, A. E.; Berendsen, H. J. C. GROMACS: fast, flexible, and free. *J. Comput. Chem.* **2005**, *26* (16), 1701–1718.
- (42) Maier, J. A.; Martinez, C.; Kasavajhala, K.; Wickstrom, L.; Hauser, K. E.; Simmerling, C. ff14SB: Improving the Accuracy of Protein Side Chain and Backbone Parameters from ff99SB. *J. Chem. Theory Comput.* **2015**, *11* (8), 3696–3713.
- (43) Brandenburg, J. G.; Bannwarth, C.; Hansen, A.; Grimme, S. B97–3c: A revised low-cost variant of the B97-D density functional method. *J. Chem. Phys.* **2018**, *148* (6), 064104.
- (44) Schauerperl, M.; Nerenberg, P. S.; Jang, H.; Wang, L. P.; Bayly, C. I.; Mobley, D. L.; Gilson, M. K. Non-bonded force field model with advanced restrained electrostatic potential charges (RESP2). *Commun. Chem.* **2020**, *3*, 44.
- (45) Lu, T.; Chen, F. Multiwfn: a multifunctional wavefunction analyzer. *J. Comput. Chem.* **2012**, *33* (5), 580–592.
- (46) Wang, J.; Wolf, R. M.; Caldwell, J. W.; Kollman, P. A.; Case, D. A. Development and testing of a general amber force field. *J. Comput. Chem.* **2004**, *25* (9), 1157–1174.
- (47) Kagami, L.; Wilter, A.; Diaz, A.; Vranken, W. The ACPYPE web server for small-molecule MD topology generation. *Bioinformatics* **2023**, *39* (6), btad350.
- (48) Jorgensen, W. L.; Chandrasekhar, J.; Madura, J. D.; Impey, R. W.; Klein, M. L. Comparison of simple potential functions for simulating liquid water. *J. Chem. Phys.* **1983**, *79* (2), 926–935.
- (49) Weber, W.; Hünenberger, P. H.; McCammon, J. A. Molecular dynamics simulations of a polyaniline octapeptide under Ewald boundary conditions: Influence of artificial periodicity on peptide conformation. *J. Phys. Chem. B* **2000**, *104* (15), 3668–3675.
- (50) Berendsen, H. J.; Postma, J. V.; Van Gunsteren, W. F.; DiNola, A.; Haak, J. R. Molecular dynamics with coupling to an external bath. *J. Chem. Phys.* **1984**, *81* (8), 3684–3690.
- (51) Hess, B.; Bekker, H.; Berendsen, H. J. C.; Fraaije, J. G. E. M. LINCS: A linear constraint solver for molecular simulations. *J. Comput. Chem.* **1997**, *18* (12), 1463–1472.
- (52) Valdés-Tresanco, M. S.; Valdés-Tresanco, M. E.; Valiente, P. A.; Moreno, E. gmx MMPBSA: A New Tool to Perform End-State Free Energy Calculations with GROMACS. *J. Chem. Theory Comput.* **2021**, *17* (10), 6281–6291.
- (53) Nguyen, H.; Pérez, A.; Bermeo, S.; Simmerling, C. Refinement of Generalized Born Implicit Solvation Parameters for Nucleic Acids and Their Complexes with Proteins. *J. Chem. Theory Comput.* **2015**, *11* (8), 3714–3728.
- (54) Pires, D. E.; Blundell, T. L.; Ascher, D. B. pkCSM: Predicting Small-Molecule Pharmacokinetic and Toxicity Properties Using Graph-Based Signatures. *J. Med. Chem.* **2015**, *58* (9), 4066–4072.
- (55) Liu, J.; Zhang, L.; Gao, J.; Zhang, B.; Liu, X.; Yang, N.; Liu, X.; Liu, X.; Cheng, Y. Discovery of genistein derivatives as potential SARS-CoV-2 main protease inhibitors by virtual screening, molecular dynamics simulations and ADMET analysis. *Front. Pharmacol.* **2022**, *13*, 961154.
- (56) National Research Council Committee for the Update of the Guide for the Care and Use of Laboratory Animals. The National Academies Collection: reports funded by National Institutes of Health. In *Guide for the Care and Use of Laboratory Animals*; National Academies Press (US): 2011.
- (57) Keihanian, F.; Moohebati, M.; Saeidinia, A.; Mohajeri, S. A.; Madaeni, S. Therapeutic effects of medicinal plants on isoproterenol-induced heart failure in rats. *Biomed. Pharmacother.* **2021**, *134*, 111101.
- (58) Hanif, W.; Alex, L.; Su, Y.; Shinde, A. V.; Russo, I.; Li, N.; Frangogiannis, N. G. Left atrial remodeling, hypertrophy, and fibrosis in mouse models of heart failure. *Cardiovasc. Pathol.* **2017**, *30*, 27–37.
- (59) Oka, T.; Akazawa, H.; Naito, A. T.; Komuro, I. Angiogenesis and cardiac hypertrophy: maintenance of cardiac function and causative roles in heart failure. *Circ. Res.* **2014**, *114* (3), 565–571.
- (60) Sun, B.; Xia, Q.; Gao, Z. Total Flavones of *Choerospondias axillaris* Attenuate Cardiac Dysfunction and Myocardial Interstitial Fibrosis by Modulating NF- $\kappa$ B Signaling Pathway. *Cardiovasc. Toxicol.* **2015**, *15* (3), 283–289.
- (61) Chi, M.; Wang, H.; Yan, Z.; Cao, L.; Gao, X.; Qin, K. Magnetic Ligand Fishing Using Immobilized Cyclooxygenase-2 for Identification and Screening of Anticoronary Heart Disease Ligands From *Choerospondias axillaris*. *Front. Nutr.* **2022**, *8*, 794193.
- (62) Ren, J.; Fu, L.; Nile, S. H.; Zhang, J.; Kai, G. *Salvia miltiorrhiza* in Treating Cardiovascular Diseases: A Review on Its Pharmacological and Clinical Applications. *Front. Pharmacol.* **2019**, *10*, 753.
- (63) Sciarretta, S.; Forte, M.; Frati, G.; Sadoshima, J. New Insights Into the Role of mTOR Signaling in the Cardiovascular System. *Circ. Res.* **2018**, *122* (3), 489–505.
- (64) Hardt, S. E. Negative regulators of cardiac hypertrophy. *Cardiovasc. Res.* **2004**, *63* (3), 500–509.
- (65) Rose, B. A.; Force, T.; Wang, Y. Mitogen-activated protein kinase signaling in the heart: angels versus demons in a heart-breaking tale. *Physiol. Rev.* **2010**, *90* (4), 1507–1546.
- (66) Yoon, S.; Seger, R. The extracellular signal-regulated kinase: multiple substrates regulate diverse cellular functions. *Growth Factors* **2006**, *24* (1), 21–44.
- (67) Ba, L.; Gao, J.; Chen, Y.; Qi, H.; Dong, C.; Pan, H.; Zhang, Q.; Shi, P.; Song, C.; Guan, X.; et al. Allicin attenuates pathological cardiac hypertrophy by inhibiting autophagy via activation of PI3K/Akt/mTOR and MAPK/ERK/mTOR signaling pathways. *Phytomedicine* **2019**, *58*, 152765.
- (68) Bhullar, S. K.; Dhalla, N. S. Angiotensin II-Induced Signal Transduction Mechanisms for Cardiac Hypertrophy. *Cells* **2022**, *11* (21), 3336.
- (69) Shah, A. K.; Bhullar, S. K.; Elimban, V.; Dhalla, N. S. Oxidative Stress as a Mechanism for Functional Alterations in Cardiac Hypertrophy and Heart Failure. *Antioxidants* **2021**, *10* (6), 931.
- (70) Breuss, J. M.; Atanasov, A. G.; Uhrin, P. Resveratrol and Its Effects on the Vascular System. *Int. J. Mol. Sci.* **2019**, *20* (7), 1523.
- (71) Li, H.; Sureda, A.; Devkota, H. P.; Pittalà, V.; Barreca, D.; Silva, A. S.; Tewari, D.; Xu, S.; Nabavi, S. M. The golden spice in treating cardiovascular diseases. *Biotechnol. Adv.* **2020**, *38*, 107343.
- (72) Hollingsworth, S. A.; Dror, R. O. Molecular Dynamics Simulation for All. *Neuron* **2018**, *99* (6), 1129–1143.
- (73) Luo, Z.; Huang, J.; Li, E.; He, X.; Meng, Q.; Huang, X.; Shen, X.; Yan, C. An Integrated Pharmacology-Based Strategy to Investigate the Potential Mechanism of Xiebai San in Treating Pediatric Pneumonia. *Front. Pharmacol.* **2022**, *13*, 784729.
- (74) Han, X.; Liu, P.; Liu, M.; Wei, Z.; Fan, S.; Wang, X.; Sun, S.; Chu, L. [6]-Gingerol Ameliorates ISO-Induced Myocardial Fibrosis by Reducing Oxidative Stress, Inflammation, and Apoptosis through Inhibition of TLR4/MAPKs/NF- $\kappa$ B Pathway. *Mol. Nutr. Food Res.* **2020**, *64* (13), No. e2000003.
- (75) Wu, J.; Kong, M.; Lou, Y.; Li, L.; Yang, C.; Xu, H.; Cui, Y.; Hao, H.; Liu, Z. Simultaneous Activation of Erk1/2 and Akt Signaling is Critical for Formononetin-Induced Promotion of Endothelial Function. *Front. Pharmacol.* **2021**, *11*, 608518.